

Ultrafast laser processing of materials in environmental and biological sciences

Santiago Camacho López

Paulina Segovia Olvera

Luis Felipe Devia Cruz

Departamento de Óptica, CICESE

camachol@cicese.mx

scamacholopez@gmail.com



NUMAR-2024

25 – 28 February 2024. Varadero, CUBA

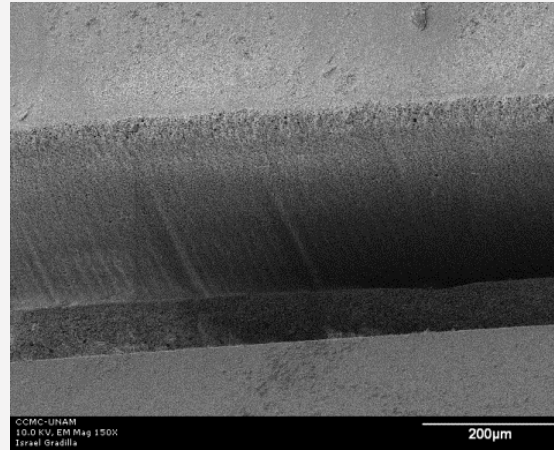
Outline

- Briefing on laser processing of materials
- Types of lasers for processing of materials
- Absorbing materials - Thermal processes
- Transparent materials – Ionization
- Laser micro/nanotexturing of surfaces
- Laser-induced cavitation
- Final remarks

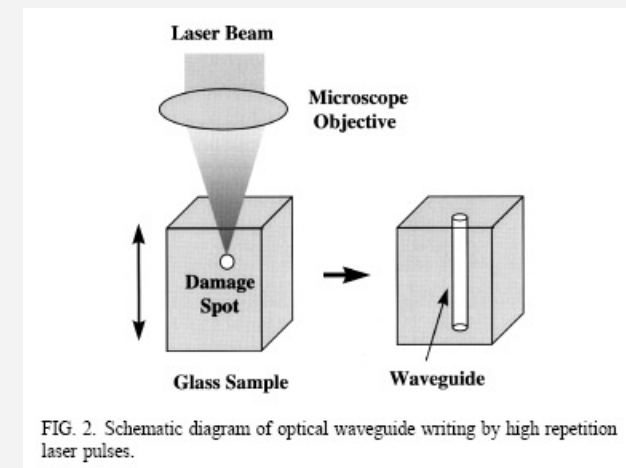
Laser processing of
materials... what does it
mean?

The laser processing of materials is the field of physics which focuses on the laser-matter interactions, aiming to understand the effects of the interaction on the material. As a result of the laser exposure, we could see some of the following:

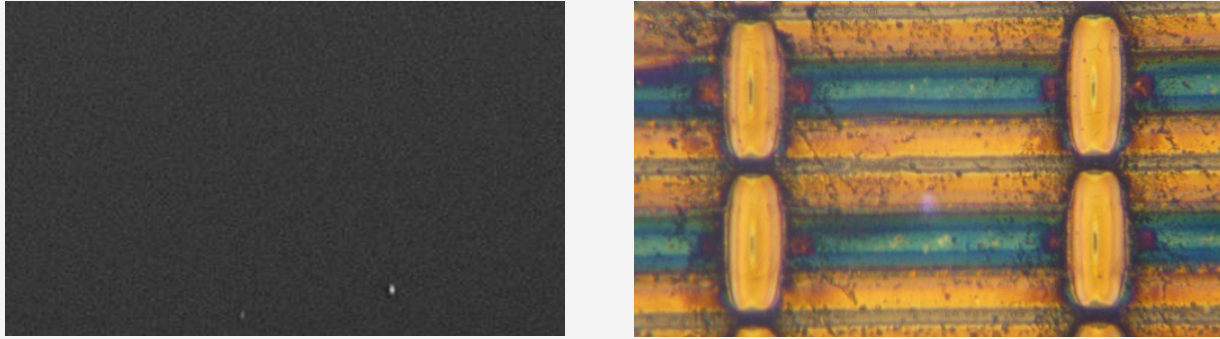
Laser ablation. Material is expelled from the surface of the sample leaving a hole behind; it leads to laser micromachining.



Laser shaping of the refractive index. In transparent materials it is possible to laser-induce a refractive index increase or decrease; it leads to waveguide formation.



Laser-induced material transformation. In several materials it is possible to laser-induce a dramatic change in the material features including their structure (crystalline, amorphous), stoichiometry, surface morphology, etc.; which leads to the modification of the optical, electrical, chemical and thermal properties.



Laser-bio interactions. Lasers are capable of selectively interacting with bio-specimens; this leads to biological and medical applications of lasers.

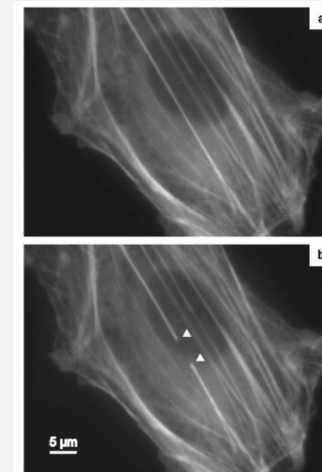
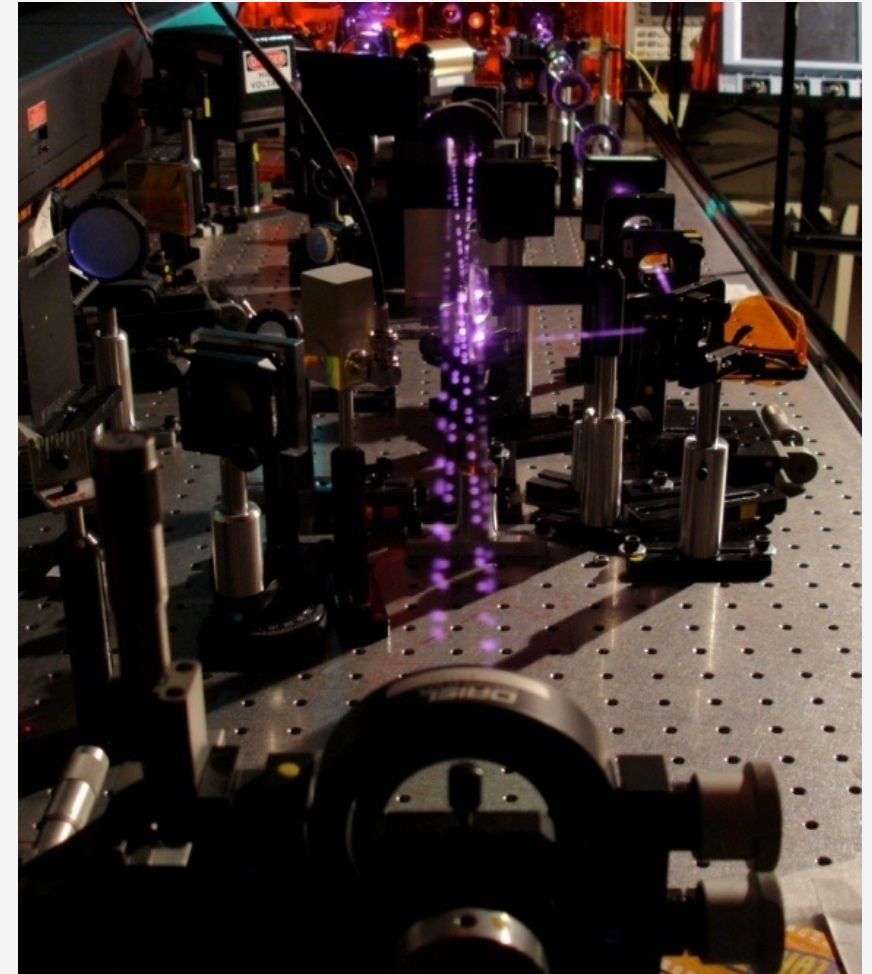
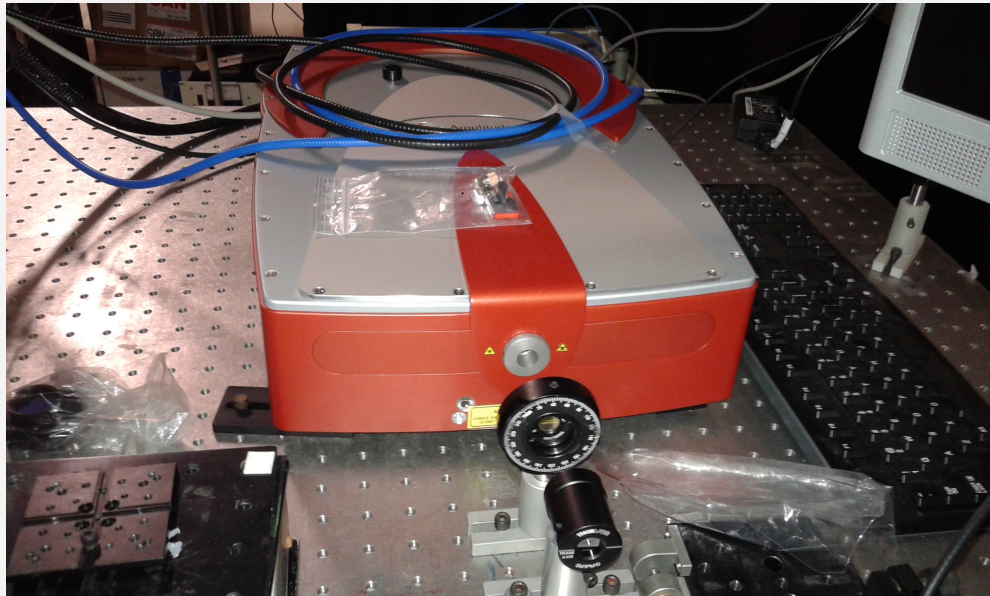


Fig. 8. Fluorescence microscope images of the YFP-labeled actin network in an endothelial cell (a) before and (b) 4 s after laser dissection of an actin fiber bundle. The triangles show the retracting ends of the bundle.

Lasers and materials meet to give place to a very interesting collection of fundamental and applied problems and challenges.

- Micro and nano-structuring of all sort of materials
- Direct laser writing waveguides in transparent materials
- 3-D patterning
- Materials physical and chemical properties modification
- Laser-biotissue interactions
- etc.



Types of lasers

Pulsed vs continuous wave (cw) lasers:

- Pulsed lasers:

Long (ms, μ s) to ultrashort pulses (femtosecond, attosecond)

Wide range of wavelengths from UV to NIR

High fluence, peak power and irradiance even for low per pulse energy

$$F = \frac{E_p}{A}; P = \frac{E_p}{\tau_p}; I = \frac{E_p}{A * \tau_p}$$

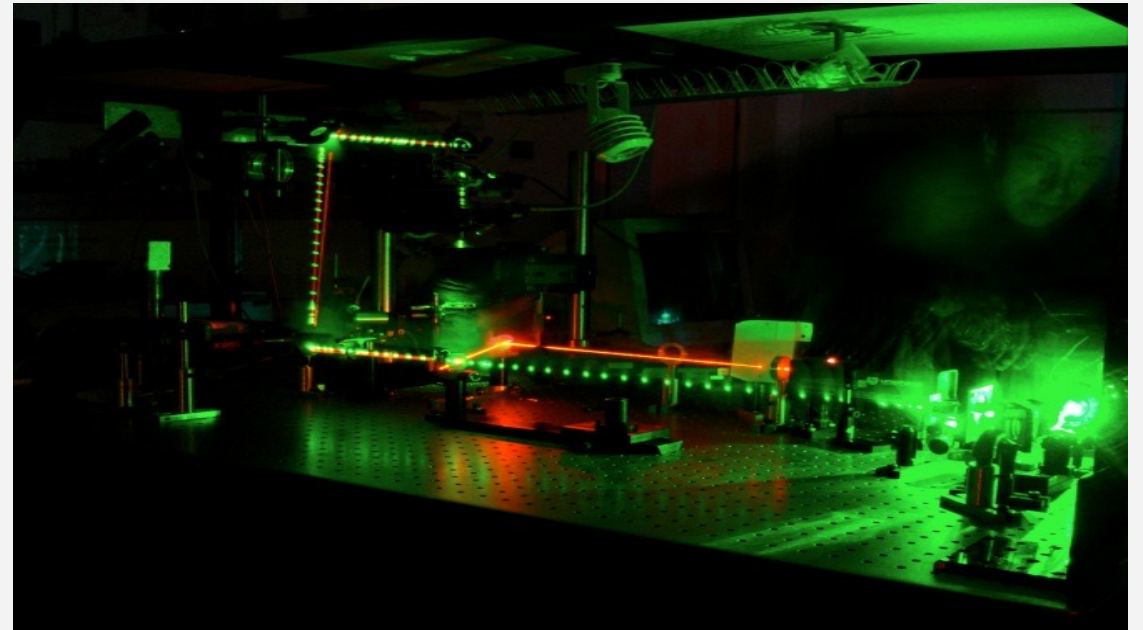
Tunable repetition rate

- CW laser:

Wide range of wavelengths from UV to NIR

High energy, moderate average power, and high fluence and irradiance possible if very tight focusing is used

Long exposures



Typical pulsed lasers for processing of materials

- Excimer

$$\lambda = 193, 308 \text{ nm}, \tau \sim 1 \text{ ns}, E_p \sim \text{mJ}, \text{Hz}$$

- Nd:YAG

$$\lambda = 1064, 532, 355 \text{ nm}, \tau \sim 5\text{-}100 \text{ ns}, E_p \sim \text{mJ}, \text{Hz-kHz}$$

- Nd:glass

$$\lambda = 1053 \text{ nm}, \tau \sim 1\text{-}10 \text{ ps}, E_p \sim \mu\text{J}, \text{Hz-kHz}$$

- Ti:sapphire

$$\lambda = 780\text{-}840 \text{ nm}, \tau \sim 50\text{-}200 \text{ fs}, E_p \sim \text{nJ}, \text{kHz-MHz}$$

- Yb fiber based

$$\lambda = 1030 \text{ nm}, \tau \sim 250 \text{ fs} - 10 \text{ ps}, E_p \sim \text{nJ}, \text{MHz}$$

Fundamental physics on the laser processing of materials

Thermal physics

Heat produced by the laser pulse train

The power density transferred to the sample by optical absorption

$$Q(r,t) = \alpha I(r,t) = \alpha \frac{2E_0 e^{-2r^2/R^2}}{\pi R^2 t_0} g(t)$$

α = Absorption coefficient [cm^{-1}]

I = Irradiance [W/cm^2]

R = Radius of laser beam

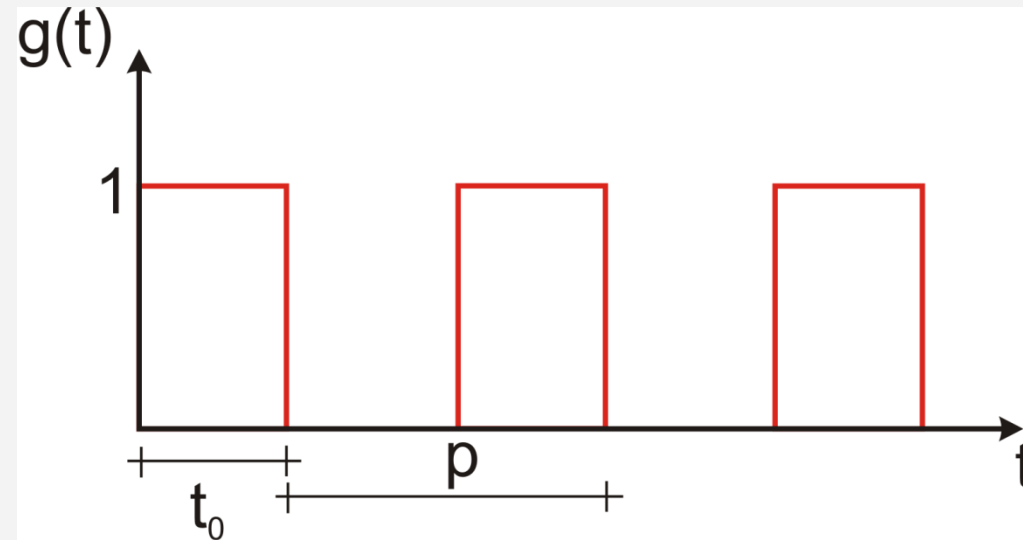
E_0 = Incident energy per pulse

t_0 = Temporal pulse width

$g(t)$ = Temporal distribution of pulse train

J. A. Sell, Photothermal investigations of solids and fluids. (Academic Press, London, 1989)

Temporal distribution of the laser pulse train



$$g(t) = \sum_{m=0}^{M-1} [H(t - mp) - H(t - (mp + t_0))]$$

M = Total number of pulses in the train

$H(t)$ = Unit step function

m = number of pulses

p = period

Heat diffusion equation

$$\frac{\partial T(r,t)}{\partial t} = D\nabla^2 T(r,t) + \frac{1}{\rho C_p} Q(r,t)$$

T = Temperature

D = Thermal diffusivity

ρ = density

C_p = specific heat at constant pressure

Boundary conditions

$$T(r,t)|_{t=0} = 0$$

$$T(r,t)|_{r=\infty} = 0$$

$$\left. \frac{dT(r,t)}{dr} \right|_{t=0} = 0$$

Temperature change due to M laser pulses

$$T(r,t) = \frac{2\alpha E_0}{\pi R^2 \rho C_p} \sum_{m=0}^{M-1} \frac{1}{\left[1 + \frac{2(t - mp)}{t_c}\right]} \text{Exp} \left[\frac{-2r^2}{R^2 \left(1 + \frac{2(t - mp)}{t_c}\right)} \right] \quad \text{for } t \geq (M-1)p$$

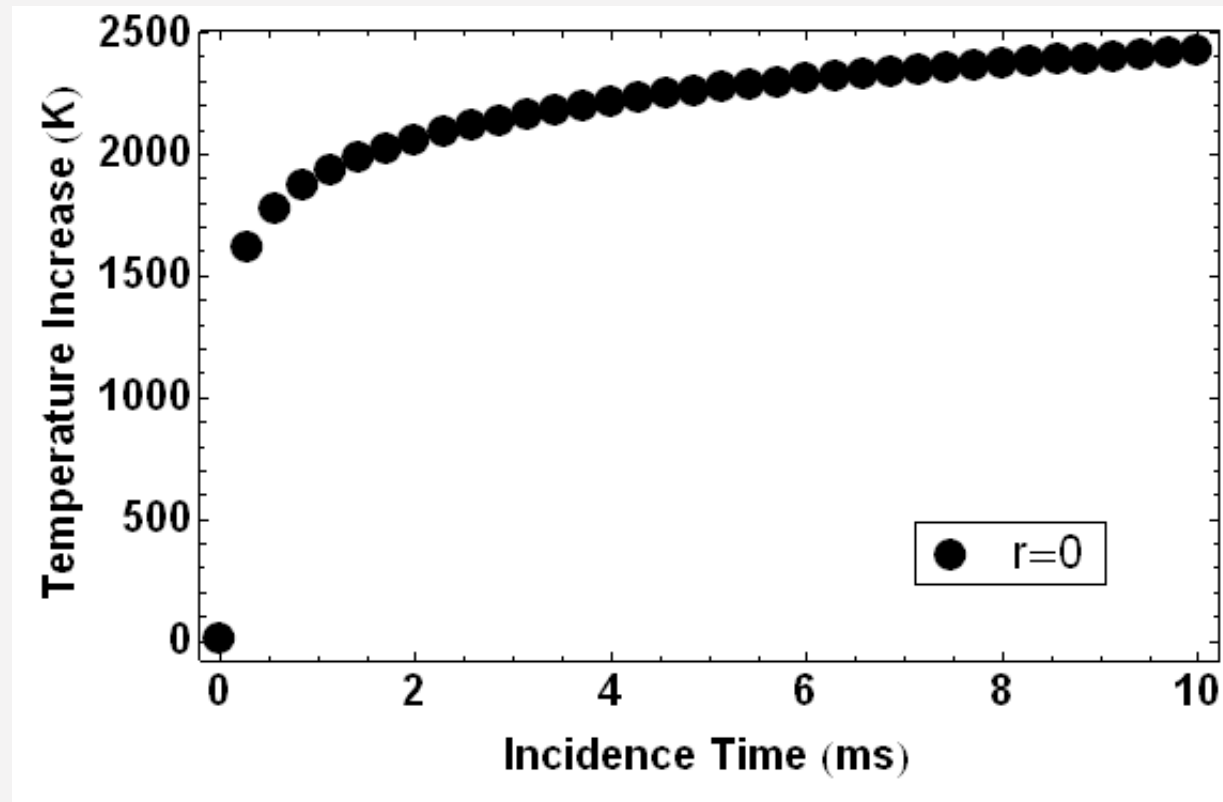
with

$$t_c = \frac{R^2}{4D} \quad R = 1.9 \mu\text{m} \quad t_c = 0.8 \mu\text{s}$$
$$D = 0.011 \text{cm}^2 \text{s}^{-1}$$

t_c = Characteristic thermal diffusion time

Temperature reached on YSZ during laser irradiation

60 fs lasers pulses at 800nm, up to 5nJ per pulse, and a rep rate of 70MHz
focusing with an aspheric lens (NA=0.5)
fluence per pulse of $\sim 30\text{mJ}/\text{cm}^2$



Nonlinear optics and ionization physics

Multiphoton ionization and avalanche ionization

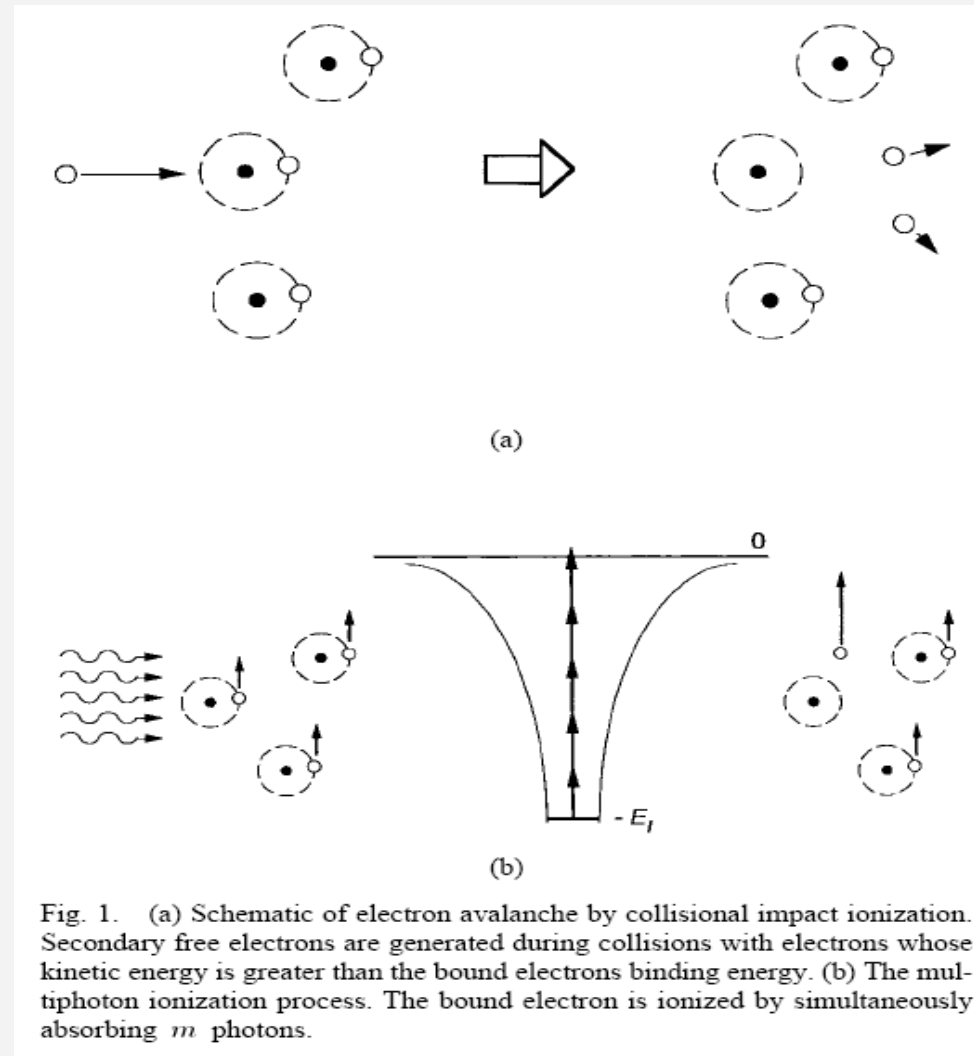


Fig. 1. (a) Schematic of electron avalanche by collisional impact ionization. Secondary free electrons are generated during collisions with electrons whose kinetic energy is greater than the bound electrons binding energy. (b) The multiphoton ionization process. The bound electron is ionized by simultaneously absorbing m photons.

Multiphoton ionization and avalanche ionization

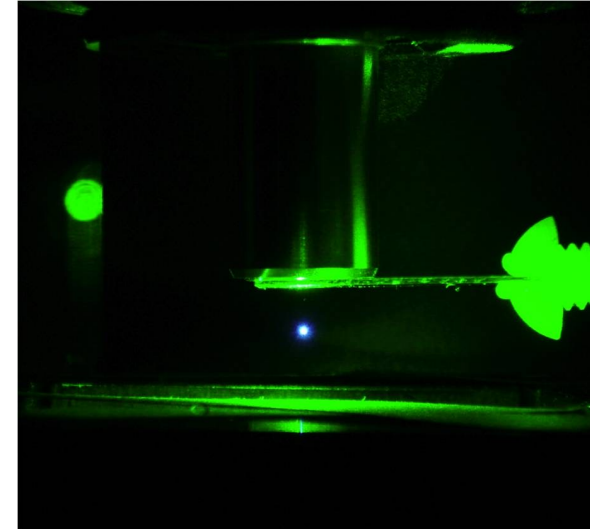
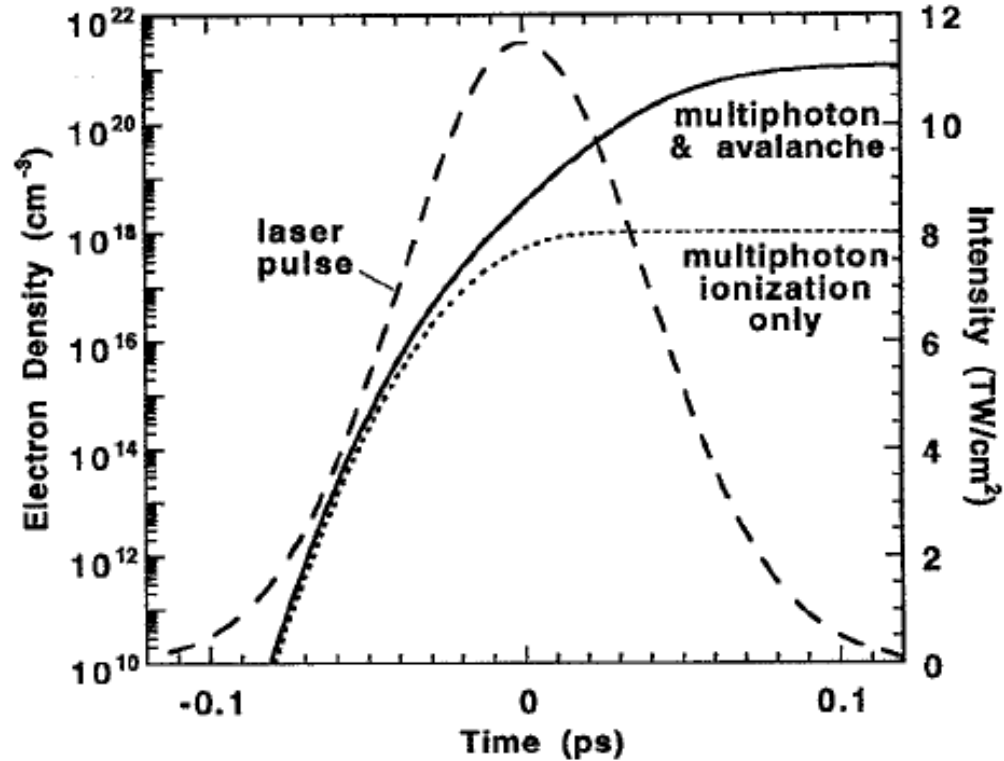
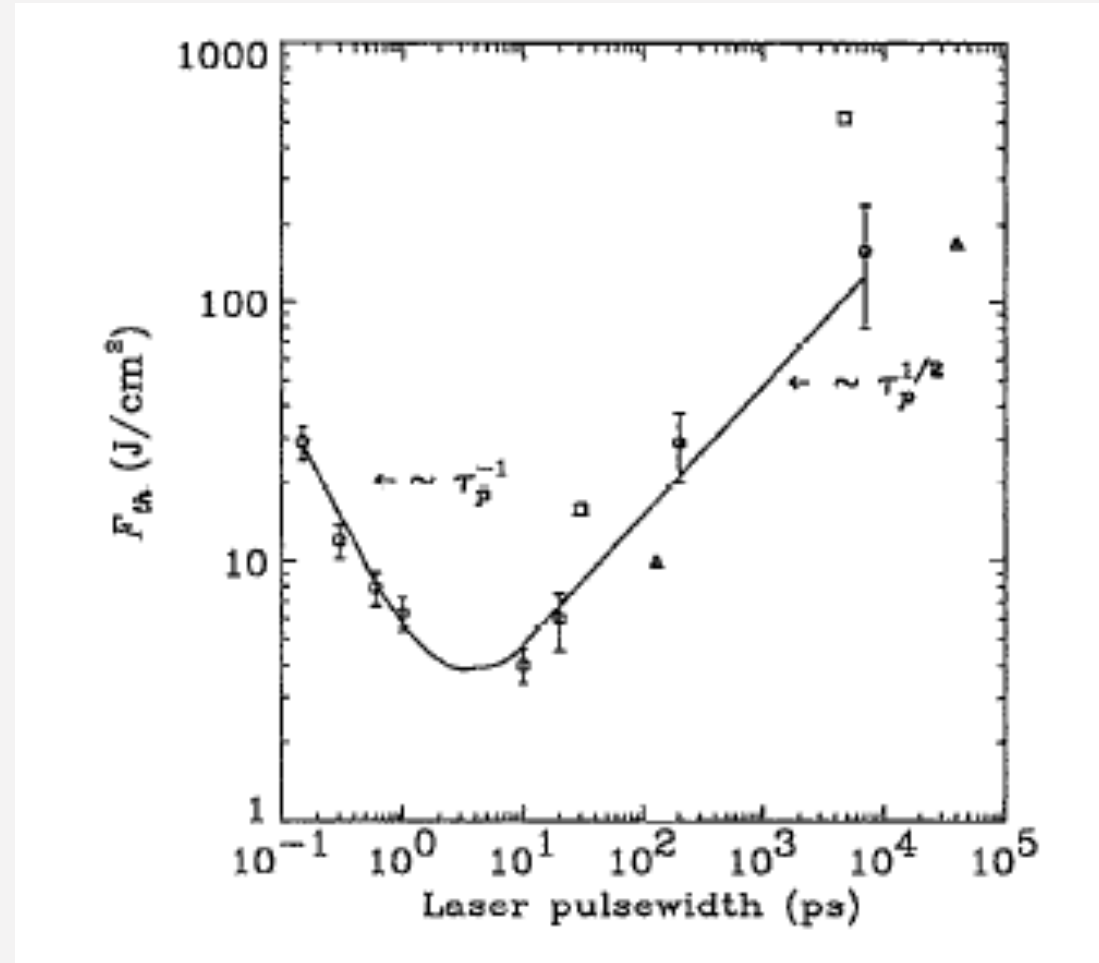


FIG. 3. Calculated evolution of free electron density for a 100 fs, 1053 nm pulse (dashed curve) of peak intensity 11.7 TW/cm^2 in fused silica. Multiphoton ionization (dotted curve) starts the avalanche; solid curve is total electron density including impact ionization.

B. C. Stuart, M. D. Feit, S. Herman, A. M. Rubenchik, B. W. Shore, and M. D. Perry, *JOSA B* **13**, 459 (1996)

Physics changes below 10 ps

Threshold laser ablation of glass vs τ_p



D. Du, X. Liu, G. Korn, J. Squier, G. Mourou. *Appl. Phys. Lett.* **64**, 3071 (1994)

Time-resolved physics

Damage for long laser pulses and damage suppression for ultrashort laser pulses

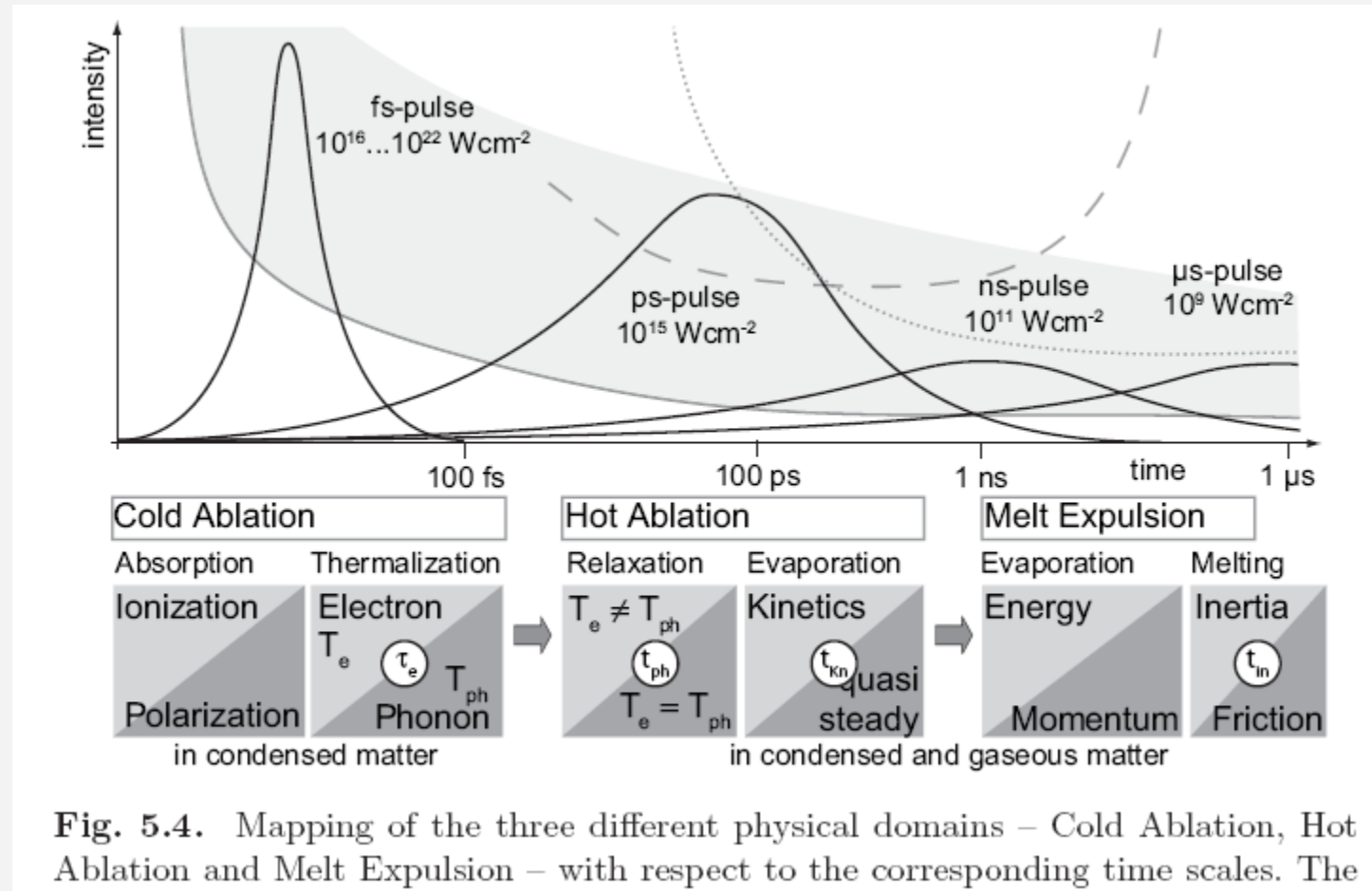
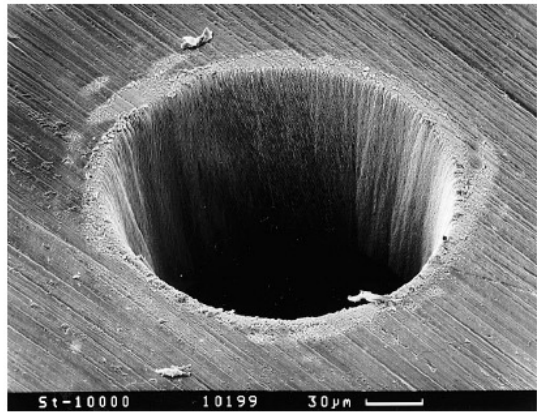
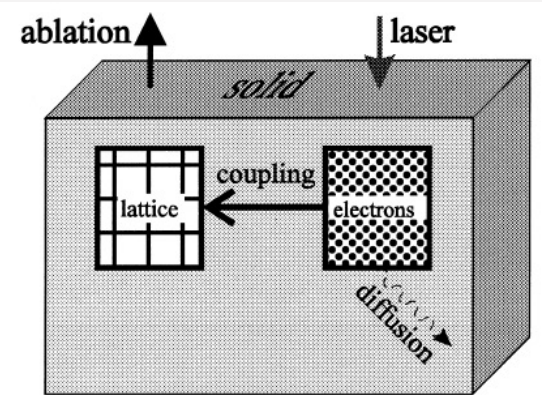
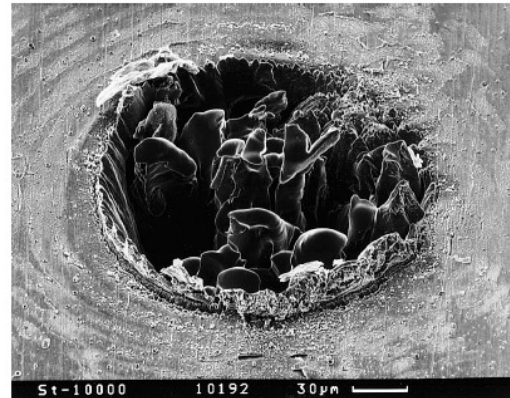
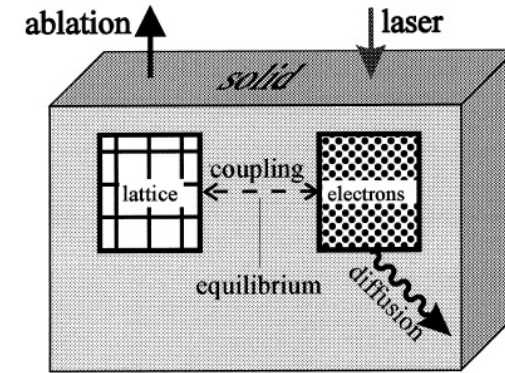


Fig. 5.4. Mapping of the three different physical domains – Cold Ablation, Hot Ablation and Melt Expulsion – with respect to the corresponding time scales. The

Laser ablation on the same material, why does it look so different?

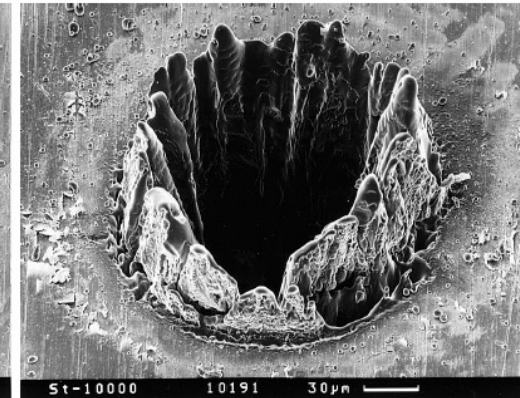


200 fs, $F = 0.5 \text{ J/cm}^2$



a

80 ps, $F = 3.7 \text{ J/cm}^2$



b

3.3 ns, $F = 4.2 \text{ J/cm}^2$

B. N. Chichkov, C. Momma, S. Nolte, F. von Alvensleben, A. Tünnermann, *Appl. Phys. A* **63**, 109 (1996)

Two-temperature model

$$C_e \frac{\partial T_e}{\partial t} = \nabla(k_e \nabla T_e) - H(T_e, T_L) + S(t)$$

$$C_L \frac{\partial T_L}{\partial t} = H(T_e, T_L)$$

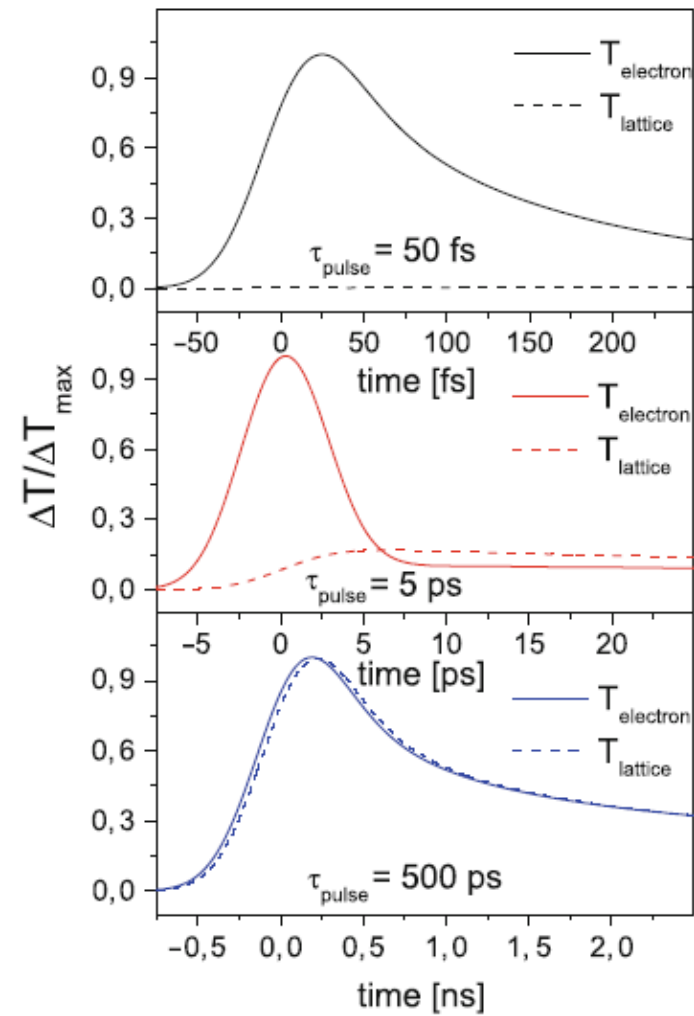
B.L. Kapeliovich, S.I. Anisimov, T.L. Perel'man, Sov. Phys. JETP 39, 375 (1975)

Electron-electron and electron-phonon interaction

26

E. Carpene et al.

Fig. 3.1 Electronic and lattice temperature profiles (simulations obtained with the TTM) in copper irradiated by laser pulses of different durations (ranging from 50 fs to 500 ps). With 50 fs pulses, electrons and lattice are completely decoupled and the lattice is substantially unaffected by the laser beam. With 500 ps pulses, electron and lattice follow almost identical temperature evolutions



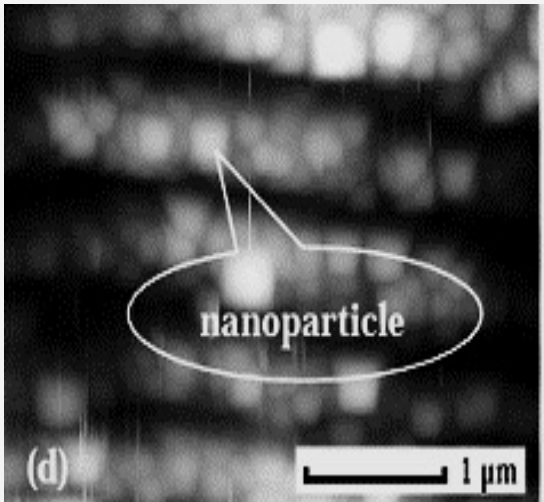
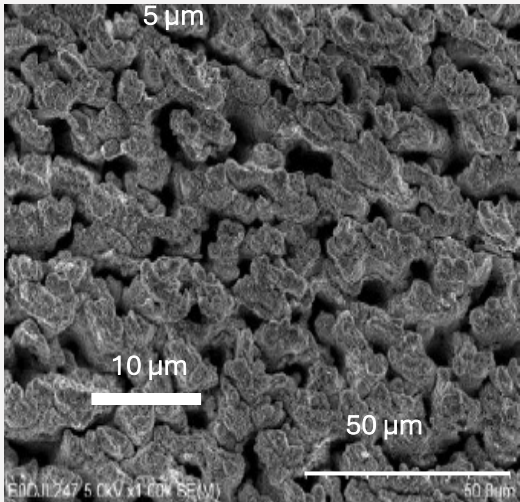
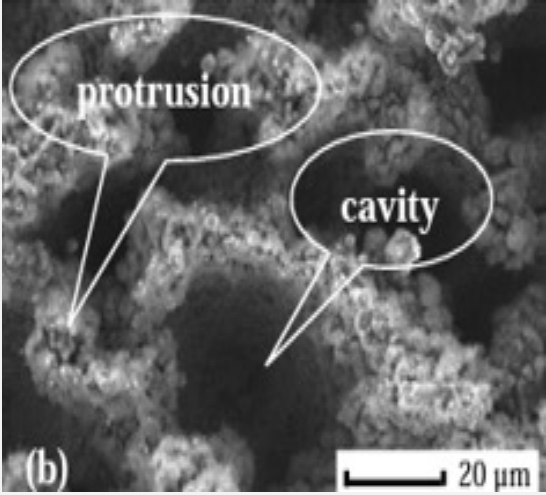
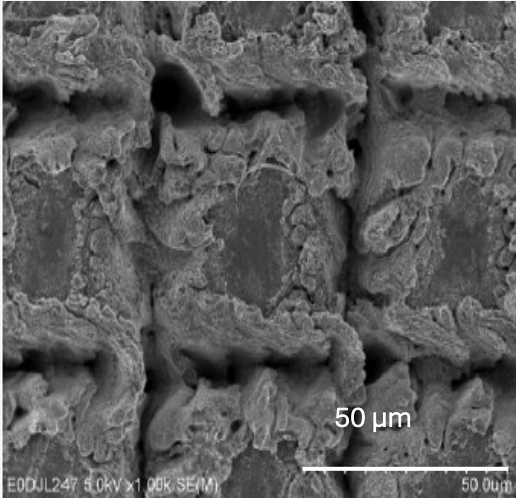
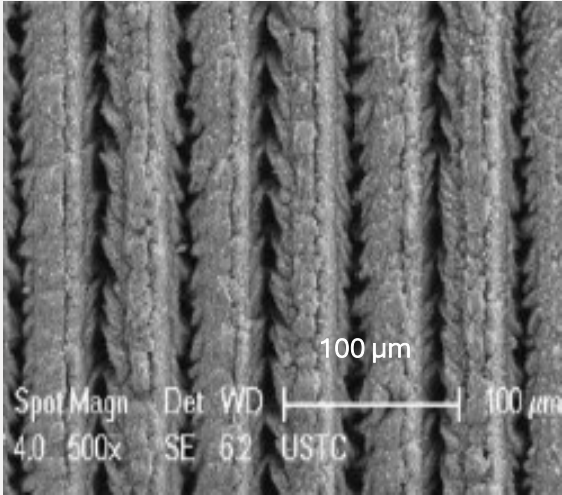
Advantages of using lasers in medicine

- Energy deposition: well controlled, and both spatial and time confined
- Optical selectivity in tissue
- Time exposure shorter than characteristic heat diffusion in biomaterials

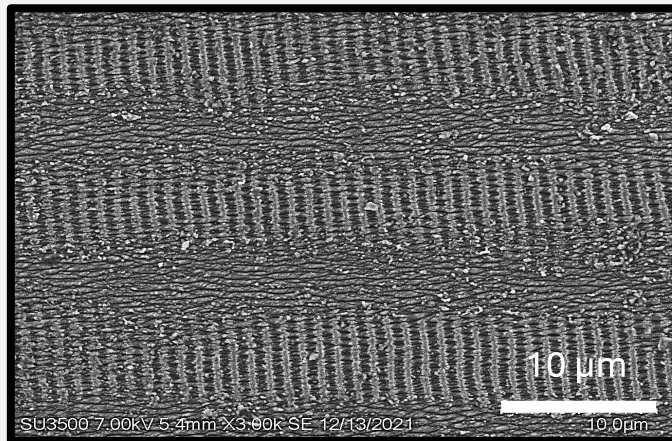
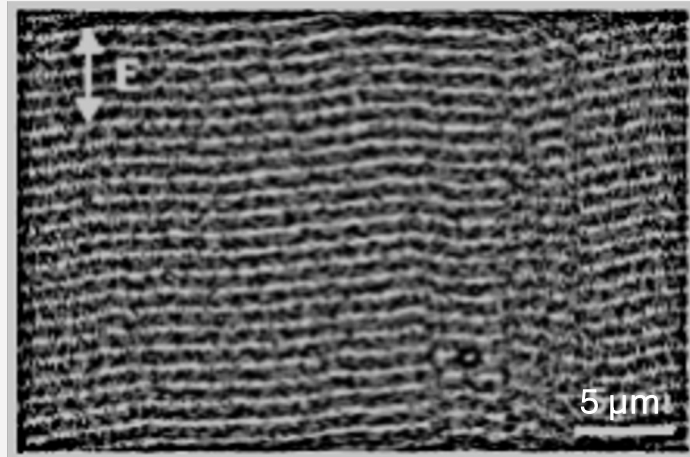
Laser micro & nano surface texturing

- **Direct Laser Ablation:** Material removal in the laser ablation process is due to the production of nanoparticles upon heating and melting the targeted material with the irradiated laser pulse.

Applied surface science 276, 203-209 (2013).

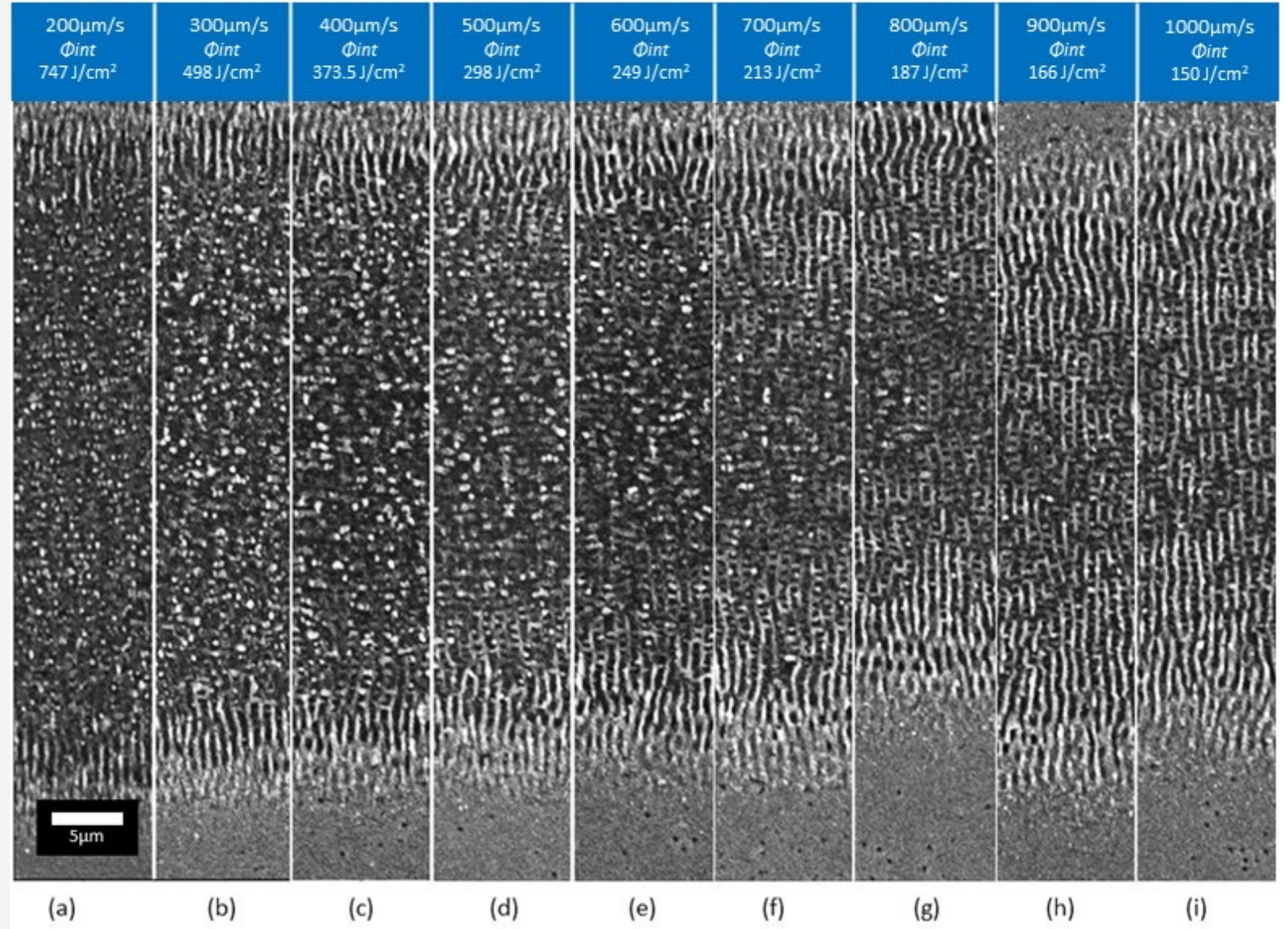


Laser Induced Periodic Surface Structures (LIPSS): self-organized micro- and nanostructures formed on the surfaces of solid material by irradiation of linearly polarized laser radiation.



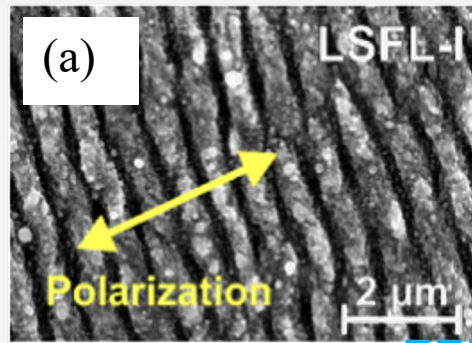
Applied Surface Science **606**, 154762 (2022).

Optical Materials Express **11**, 2892-2906 (2021).

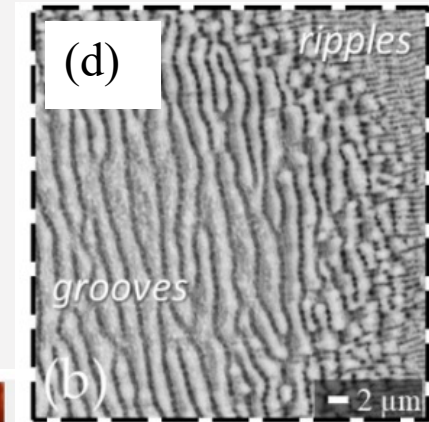
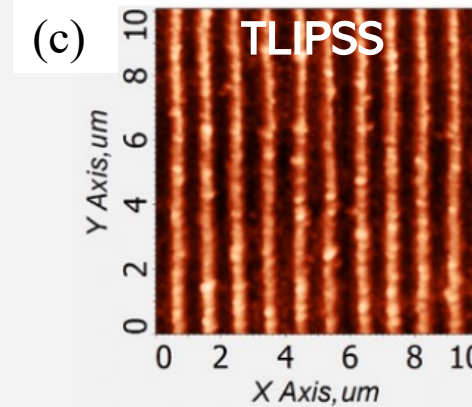
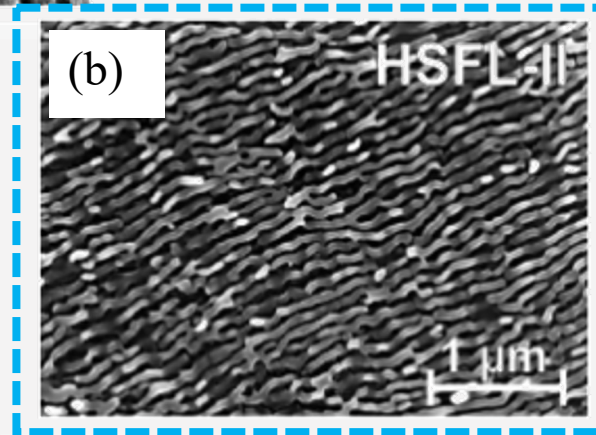


LIPSS

- Laser-induced Periodic Surface Structures.
- Universal phenomenon.
- Quasi-periodic lines.
- Simple single-step process



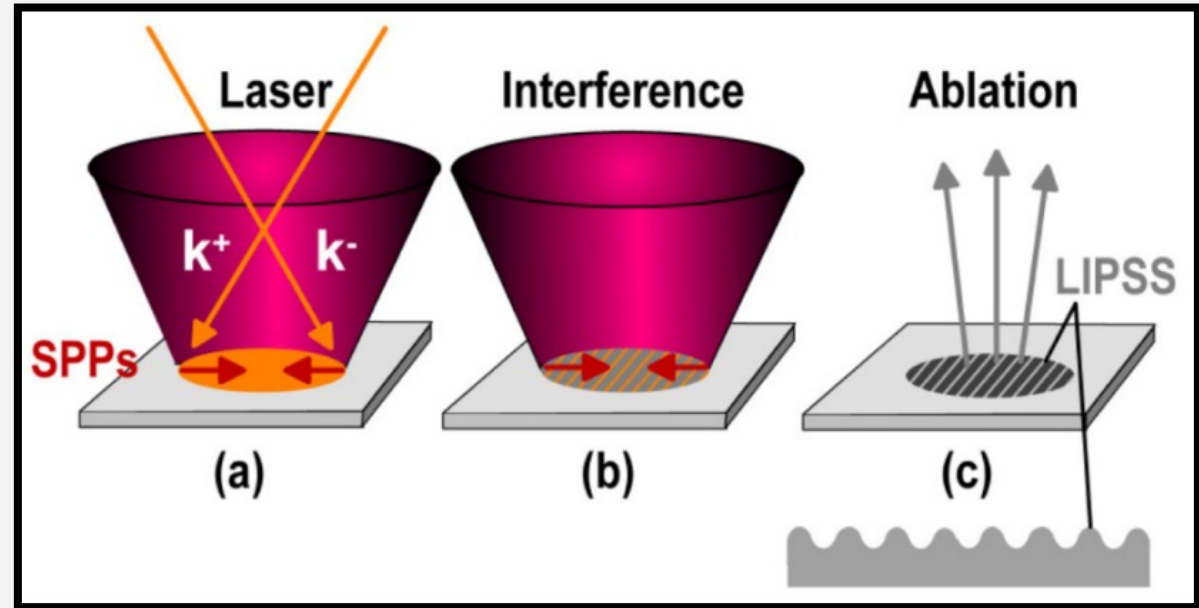
- a) Low spacial frequency LIPSS $\lambda/2 \leq \Lambda_{LSFL} \leq \lambda$.
- b) High spacial frequency LIPSS $\Lambda_{HSFL} < \lambda/2$
- c) Thermochemical LIPSS $\lambda/2 \leq \Lambda_{TL} \leq \lambda$
- d) Suprawavelength LIPSS $\Lambda_{SL} > \lambda$



- (a,b) J. Bonse, S. Höhm, S. V. Kirner, A. Rosenfeld and J. Krüger, *IEEE Journal of Selected Topics in Quantum Electronics*, **23**, 9000615, (2017).
(c) Dostovalov, A.V. & Korolkov, Victor & Terentiev, V. & Okotrub, K. & Dultsev, Fedor & Babin, Sergey. (2016).. 10.1109/PIERS.2016.7735797.
(d) Nivas JJ, Amoroso S.. *Nanomaterials* **11**, 174 (2021).

LSFL

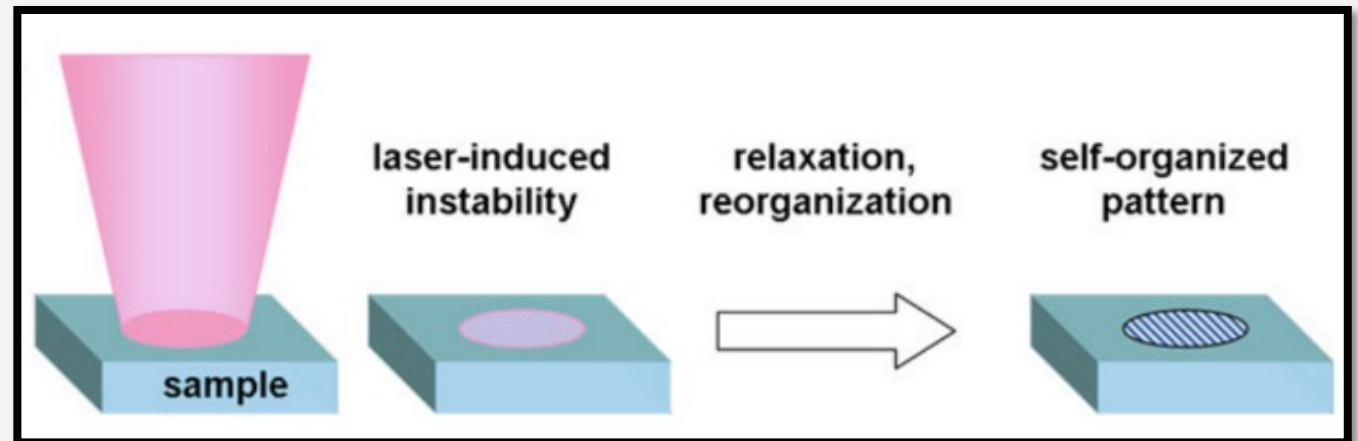
ELECTROMAGNETIC THEORIES



J. E. Sipe, et al. Physical Review B 27, 1141 (1983).

HSFL

SELF-ORGANIZATION

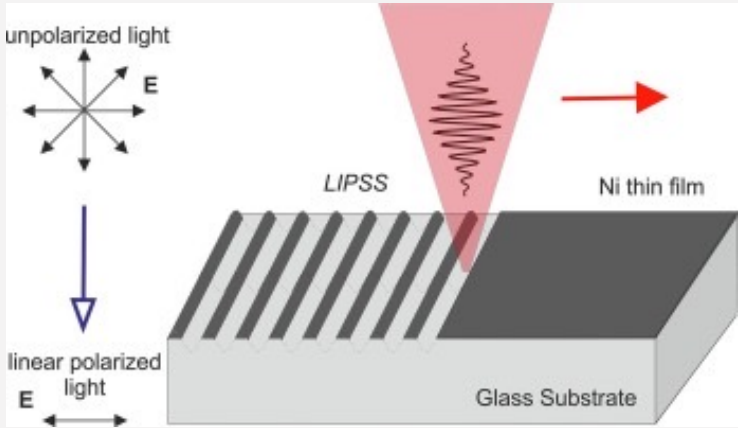
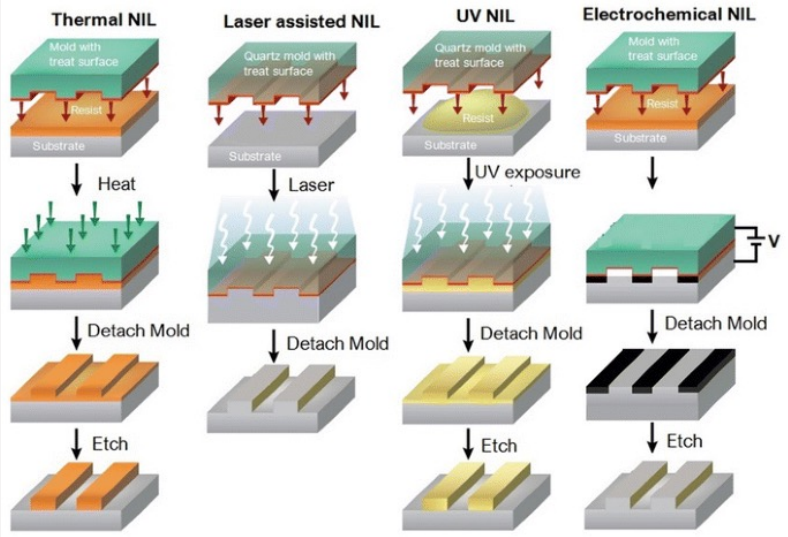


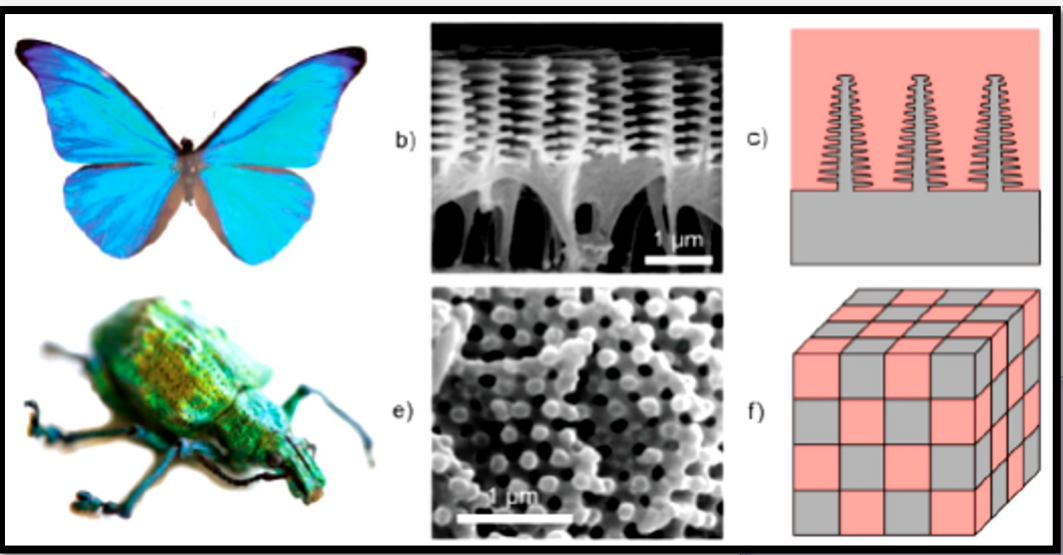
Olga Varlamova, et al. (2015). Springer International Switzerland, S. Sakabe et al. (eds.), Progress in Nonlinear Nano-Optics, Nano-Optics and Nanophotonics.

ADVANTAGES

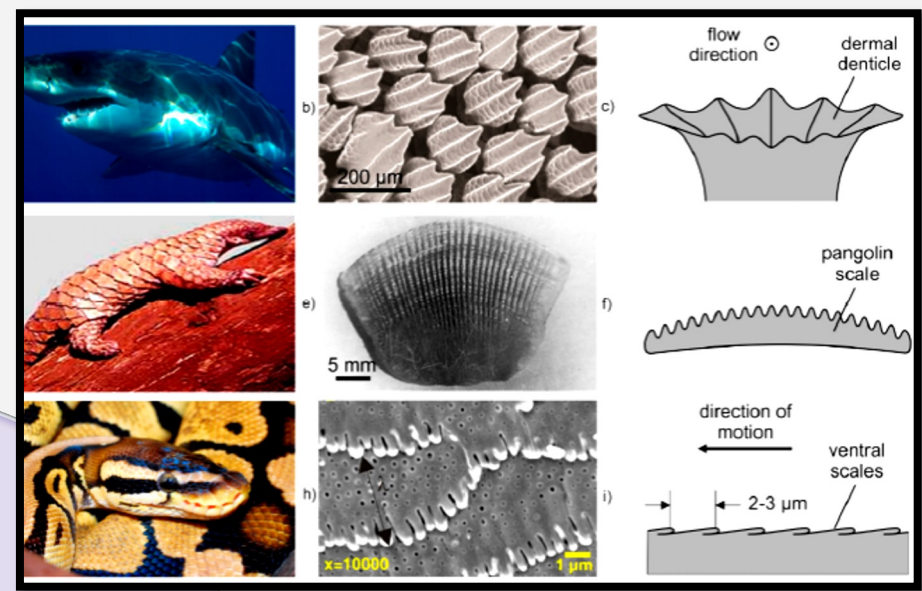
NANOLITHOGRAPHY

LASER TEXTURING



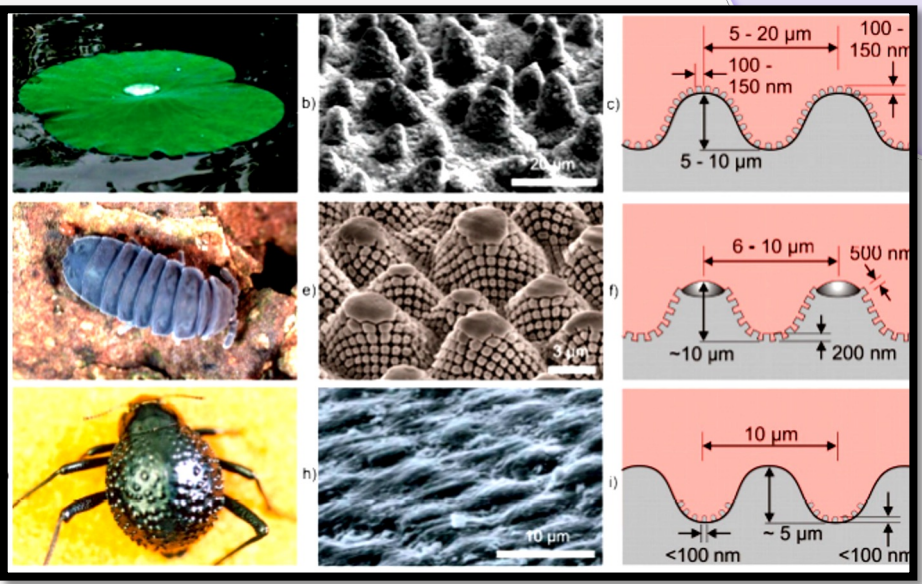


Coloring structures, Optical massive storage

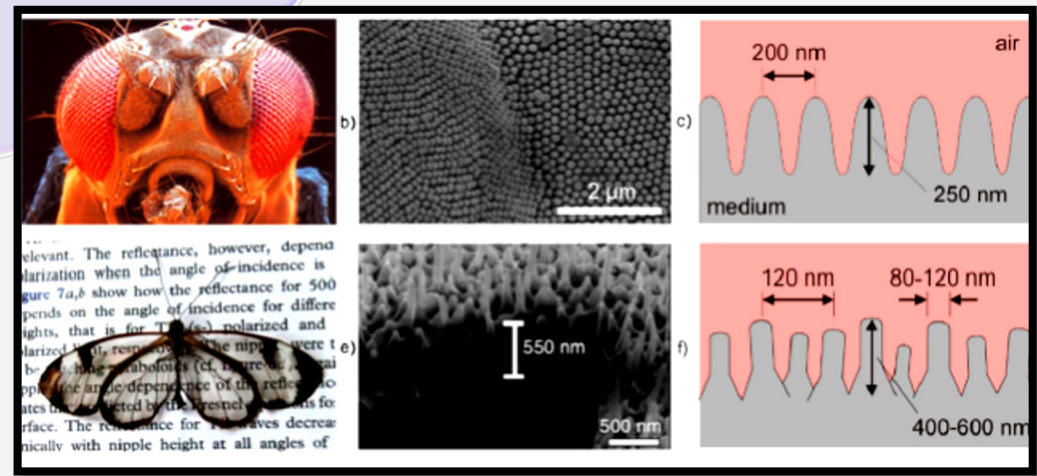


Tribological applications

APPLICATIONS



Hydrophobic applications

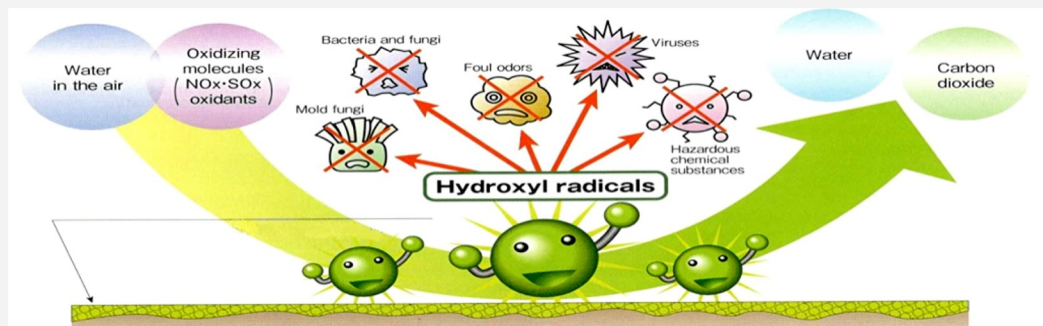
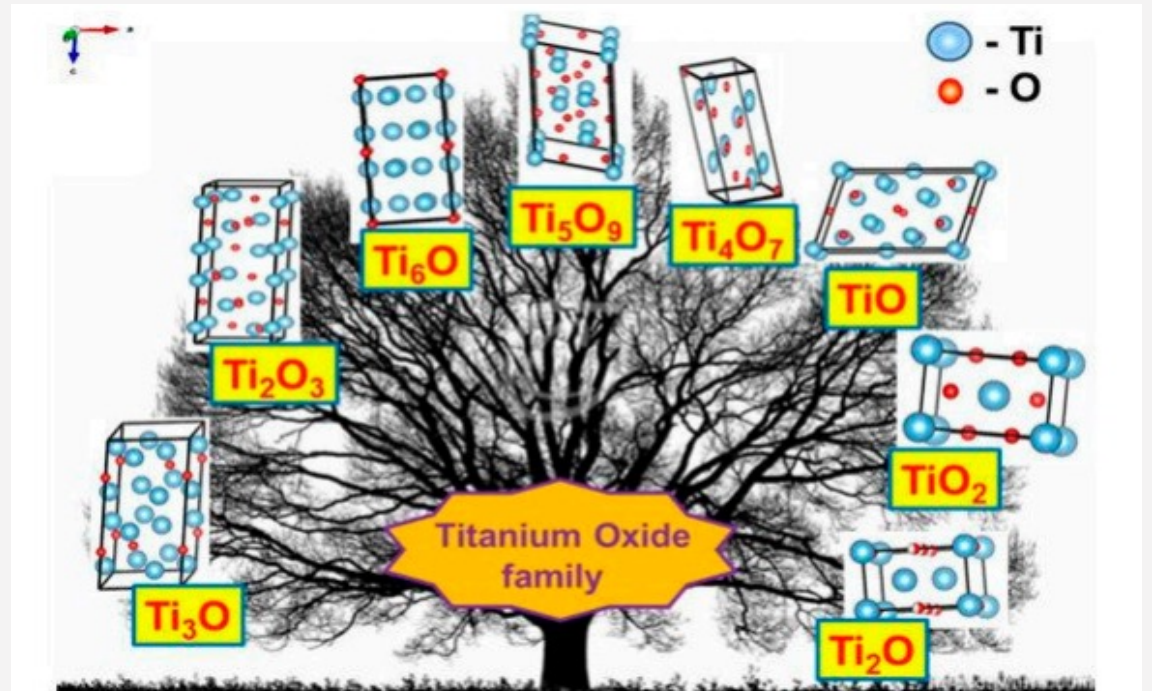
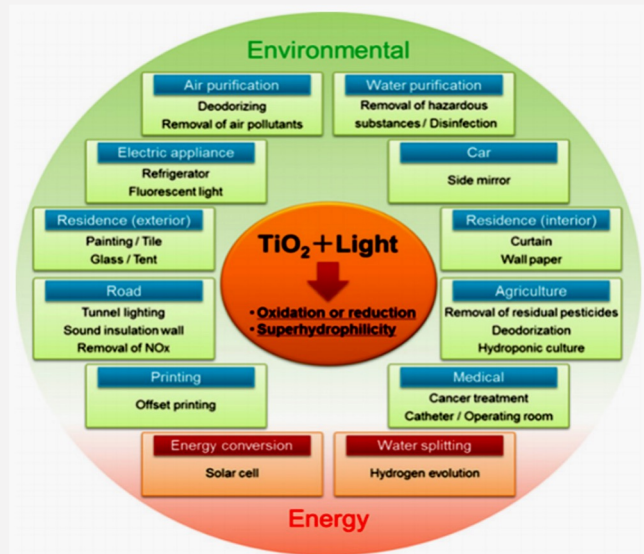


Antireflective surfaces

Muller, Kunz & Graf. *Materials* 9, 476 (2016).

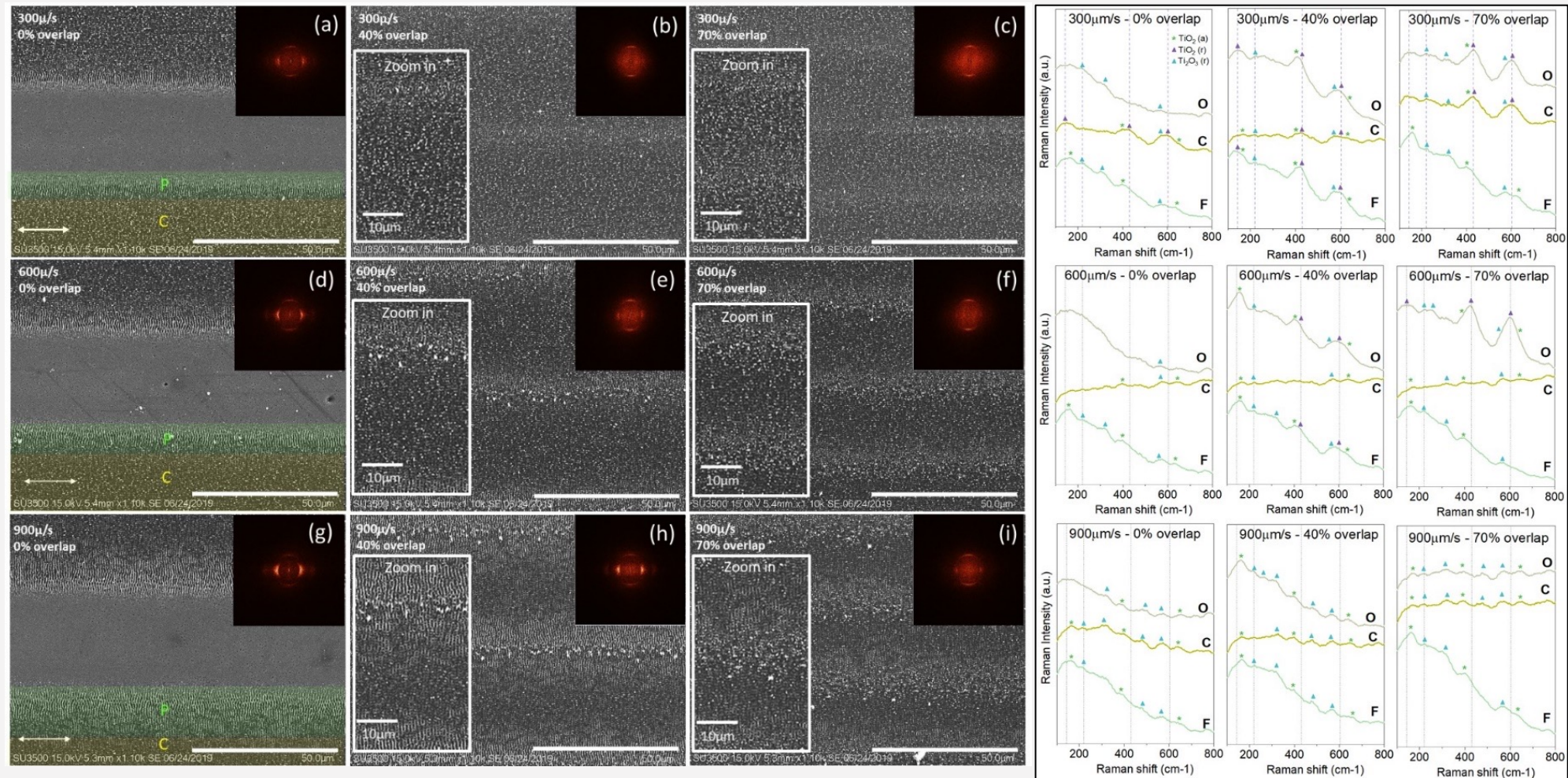
Photocatalysis / Gas sensors

TiO₂ - biocompatible, photocatalytic, metamaterial (high refractive index and also refractive index near zero)



fs-large-area fabrication of multi-phase titanium oxide LIPSS on thin films

Lamborghini Sotelo , Ricardo Santillan, Paulina Segovia Olvera , Santiago Camacho López

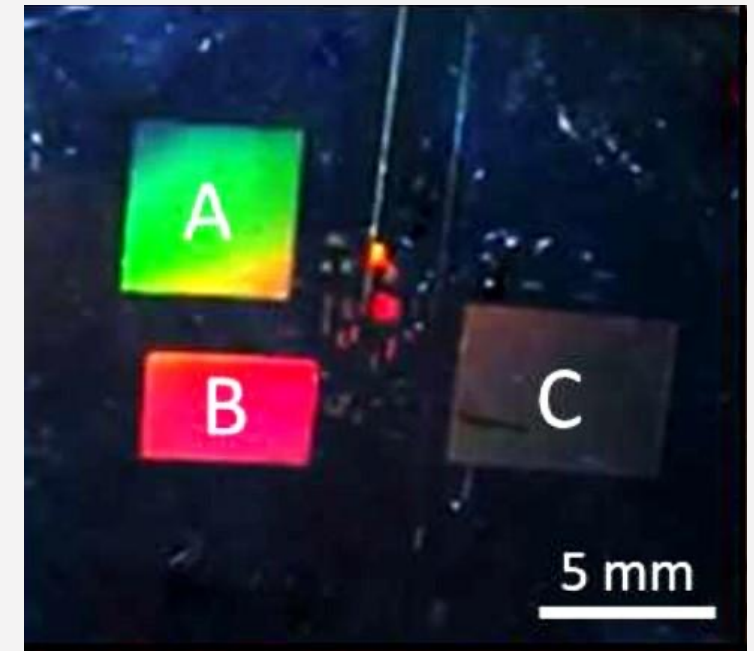
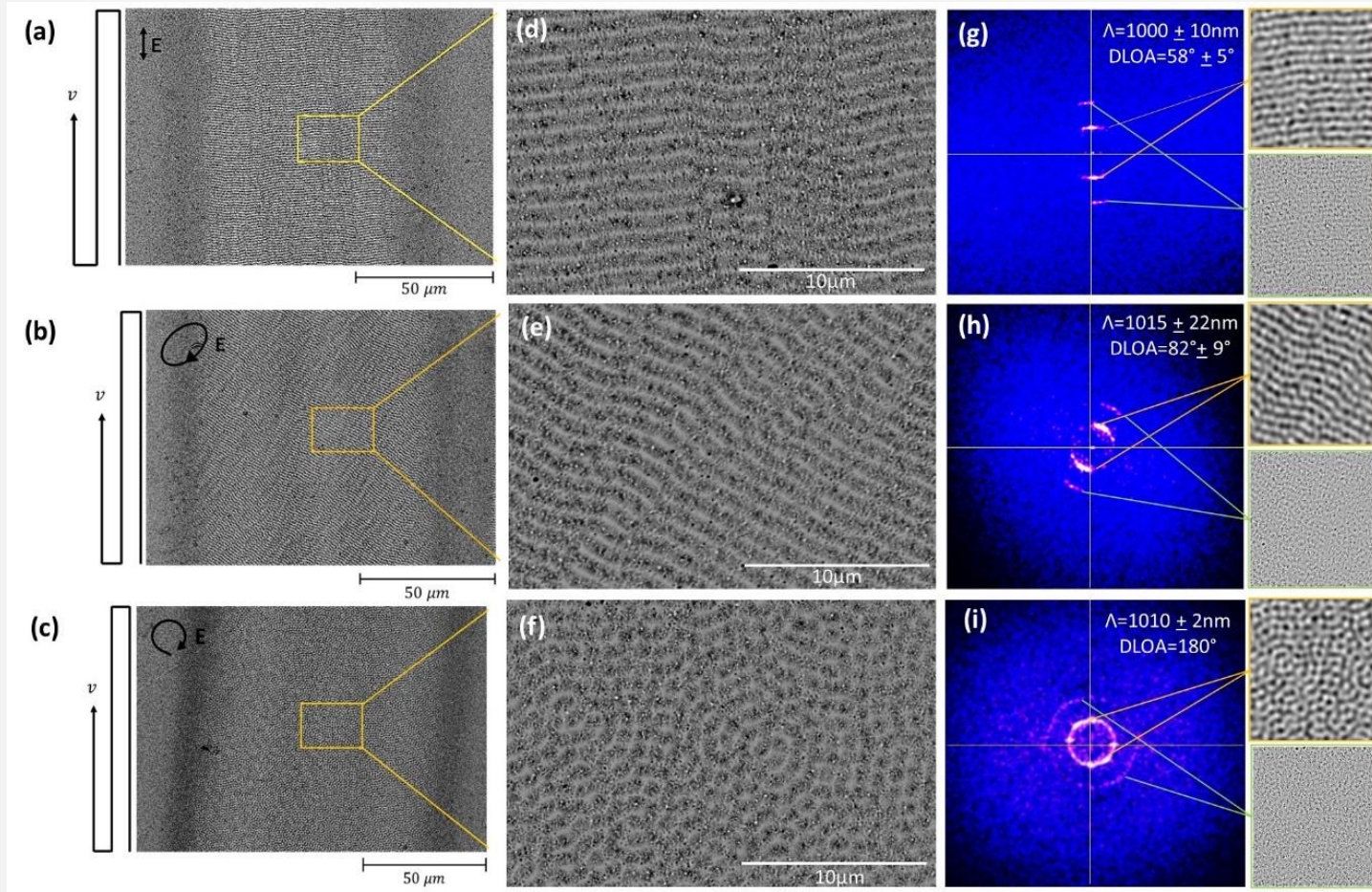


Raman spectra of the Ti film irradiated at a fluence per pulse of 116 mJ/cm² for different scanning velocities and overlap rate (0%, 40% and 70%); (a-c) 300 μm/s, (d-f) 600 μm/s, (g-i) 900 μm/s. Raman spectra were measured at different zones, overlap (O), frontier (F) and center (C).

SERS substrates/ structural colors

Design and fabrication of Bi nanostructured surfaces via LIPSS formation through Surface Plasmons

Abigail Fraijo, Paulina Segovia Olvera, Santiago Camacho López



Picture of the structured colors generated by LIPSS fabricated with linear (A), elliptical (B) and circular (C) polarized radiation

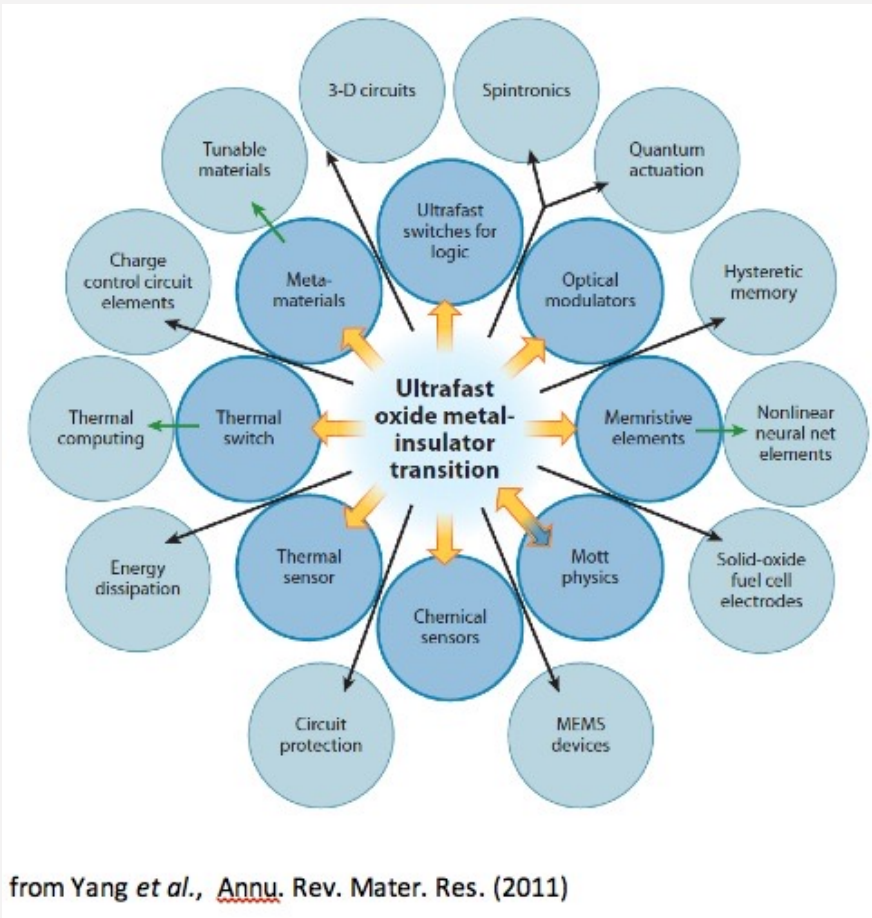
LIPSS on bismuth thin films have applications in fields like surface coloring, color coding, polarization sensitive displays, surface texturing, diffraction gratings for miniaturized spectroscopy devices, plasmonics for an spectral range from far IR to UV.

Smart materials (VO₂)

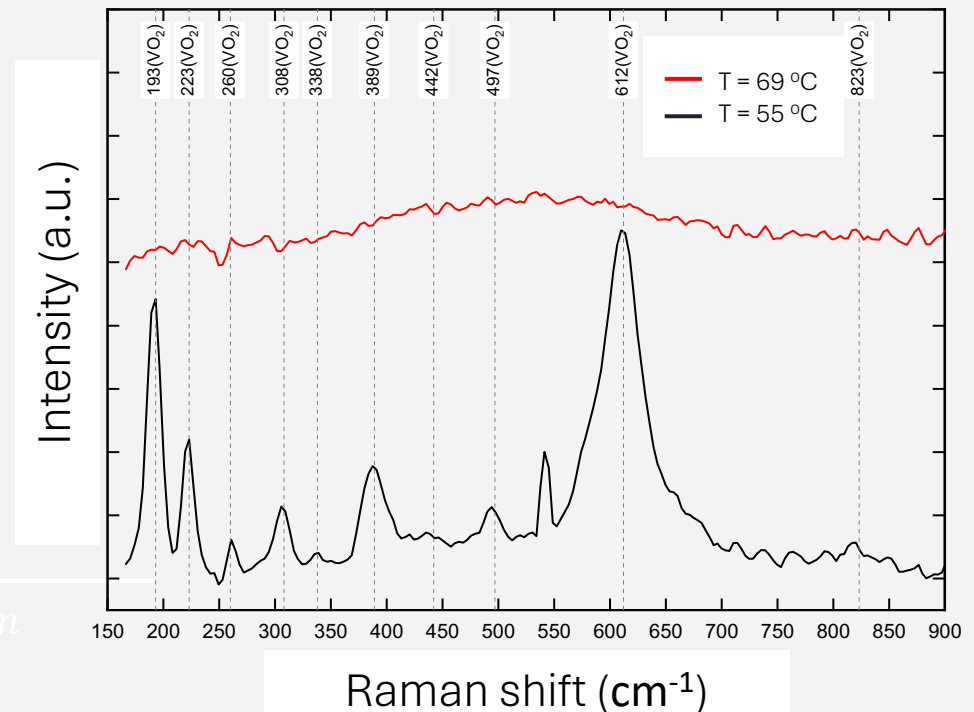
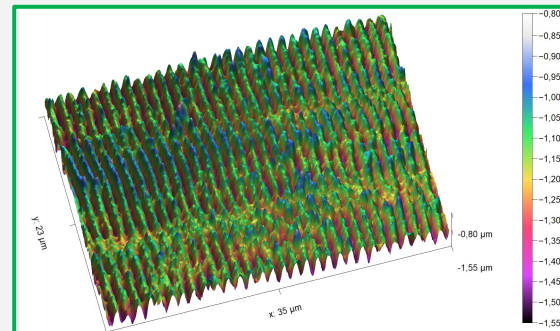
Study of fs-lipss formation on V

Noel Ramos, Paulina Segovia Olvera, Santiago Camacho López

Vanadium oxides are chromogenic materials and can change their optical properties due to some external stimuli in the form of photon radiation (photochromic), change in temperature (thermochromic), and voltage pulse (electrochromic)



$F_p = 18.5 \text{ mJ/cm}^2$
 $V_s = 3.3 \mu\text{m}$ SLIPSS VO₂ ($\Lambda_{\parallel} = 1133 \text{ nm}$)
Depth = 320 nm



Antibacterial surfaces, cell viability, adhesion and proliferation



Laser texturing of 8YSZ for skull implants

Luis Fernando Dávila González, Paulina Segovia Olvera, Ana Guadalupe Rodríguez Hernández, Santiago Camacho López

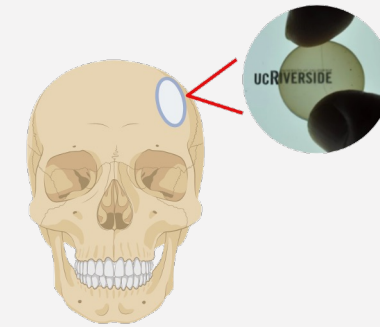
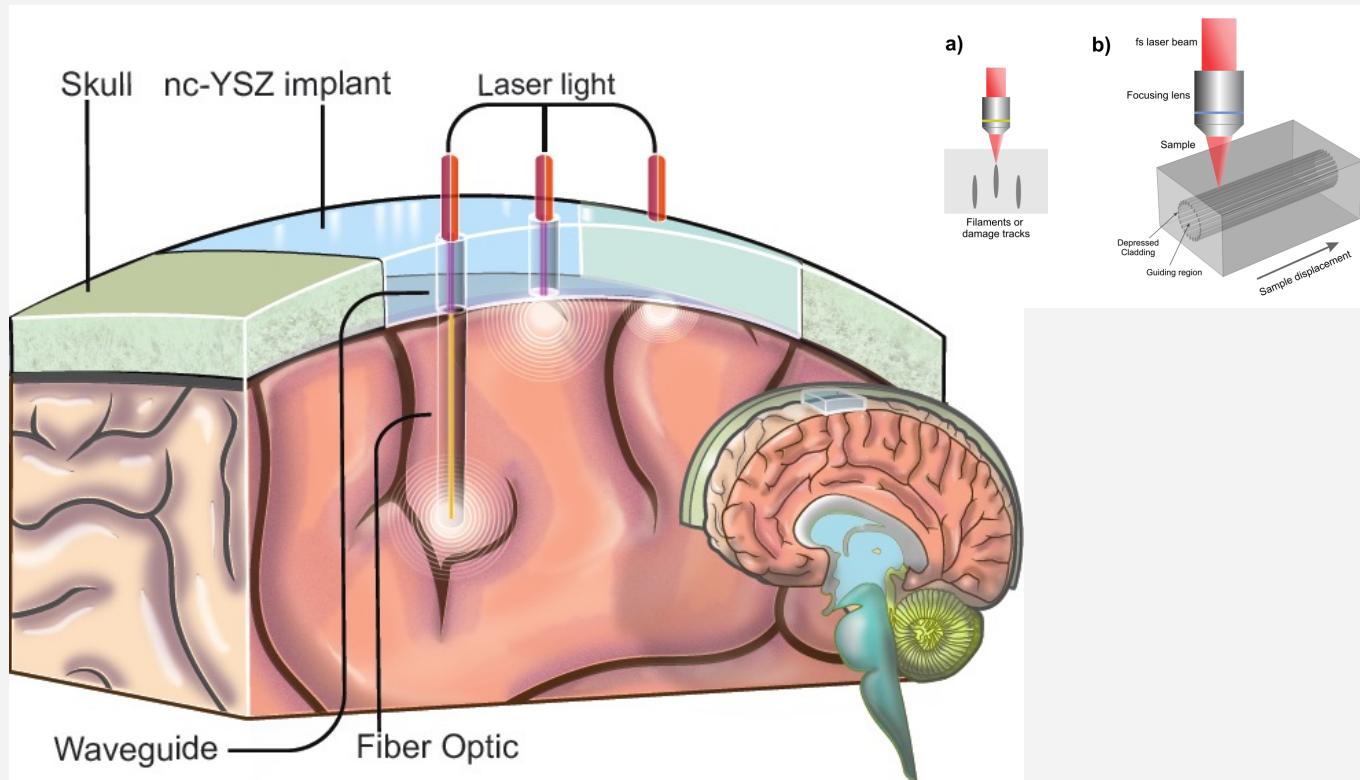
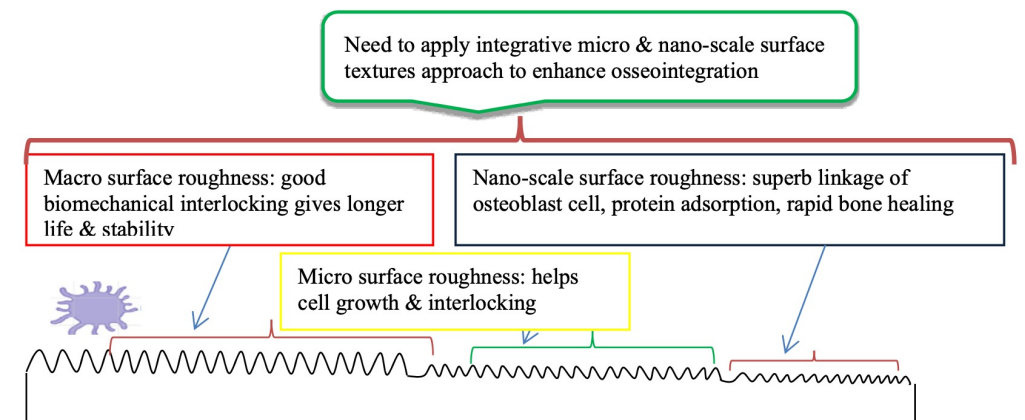


Illustration of implant with 8YSZ sample.. (UC, Riverside, 2010)

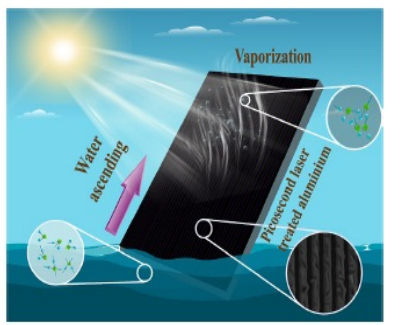


Influence of topography on the osteointegration process.(Sirdeshmukh & Dongre, 2021)

“Circular depressed cladding waveguides in mechanically robust, biocompatible nc-YSZ transparent ceramics by fs laser pulses” C. Guerra-Olvera, G. R. Castillo, E. H. Penilla, G. Uahengo, J. E. Garay, and S. Camacho-Lopez. *Journal of Lightwave Technology* **37**, 3119-3126 (2019).

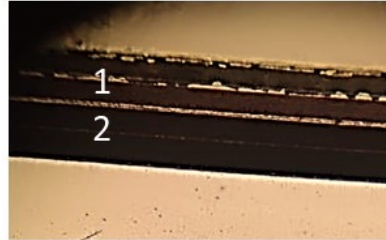
fs - laser blackening of aluminum alloy for water desalination

Leydy Velásco , Paulina Segovia Olvera, Francisco Carranza, Santiago Camacho López.



Lineal polarization

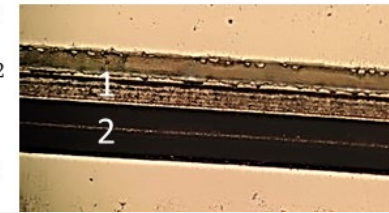
- 1 $P_{inc} = 200 \text{ mW}$
 $F_p = 0,6288 \text{ J/cm}^2$
- 2 $P_{inc} = 500 \text{ mW}$
 $F_p = 1,5719 \text{ J/cm}^2$



Light trapping microstructure and nanostructure is generated to absorb light from UV, visible to long-wave infrared spectral region.

Circular polarization

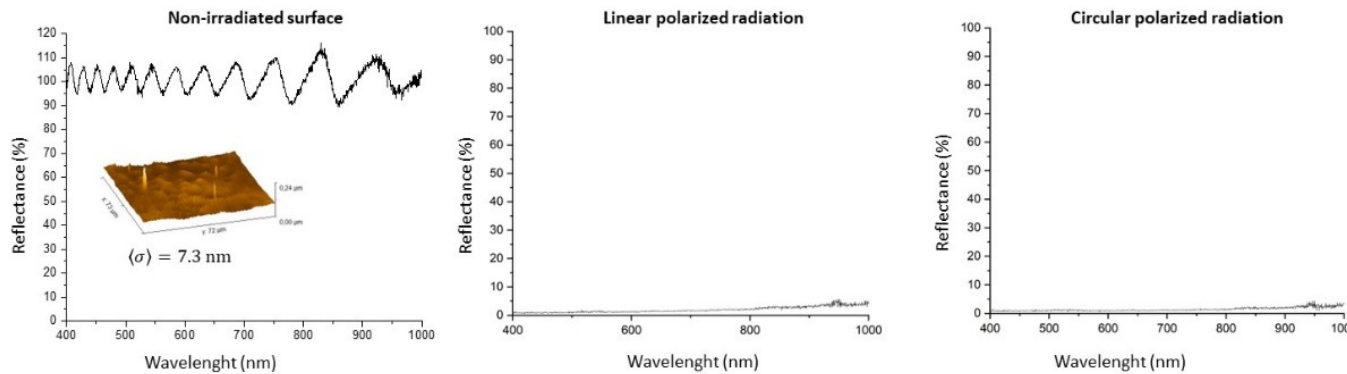
- 1 $P_{inc} = 200 \text{ mW}$
 $F_p = 0.6288 \text{ J/cm}^2$
- 2 $P_{inc} = 500 \text{ mW}$
 $F_p = 1,5719 \text{ J/cm}^2$



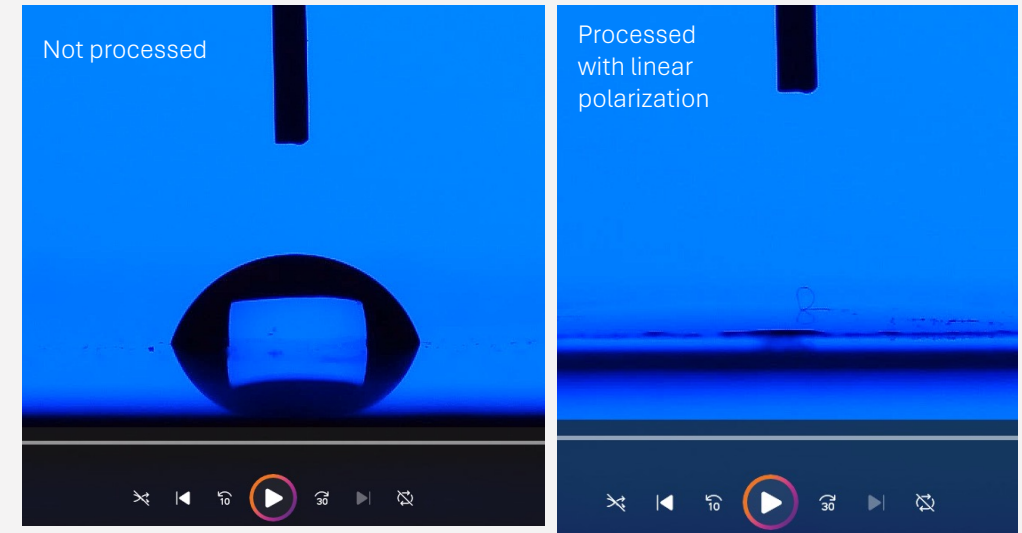
Absorption of light due to multiple reflections, excitation of surface plasmons polaritons and excitation of localized surface plasmons.

Super-blackening and hydrophilic surface

Optical Micrographs of modified aluminum surface showing different colors: brown, golden, and black.



Reflectance for Al alloy before processing and after blackening with linear and circular polarized radiation.



Modifying wettability on Al Surface.

LASER INDUCED CAVITATION BUBBLES:
STUDIES AND APPLICATIONS IN BIO AND ENVIROMENT

Cavitation occurs when $P_{\text{Fluid}} \ll P_{\text{vapor}}$

Boiling water



- Fluid Pressure \ll Vapor Pressure
(Constant)



Low pressure regions



- Fluid Pressure \ll Vapor Pressure
(Constant)



Laser induced

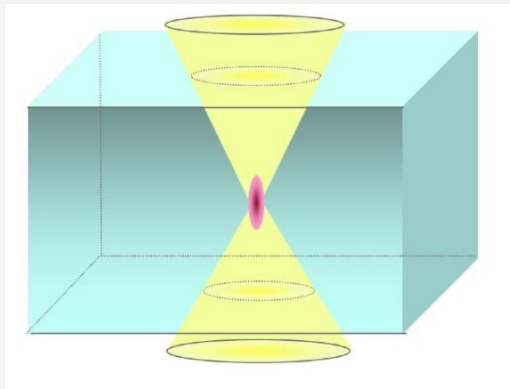


Photoionization

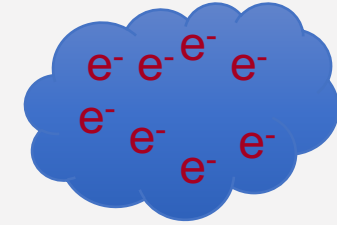
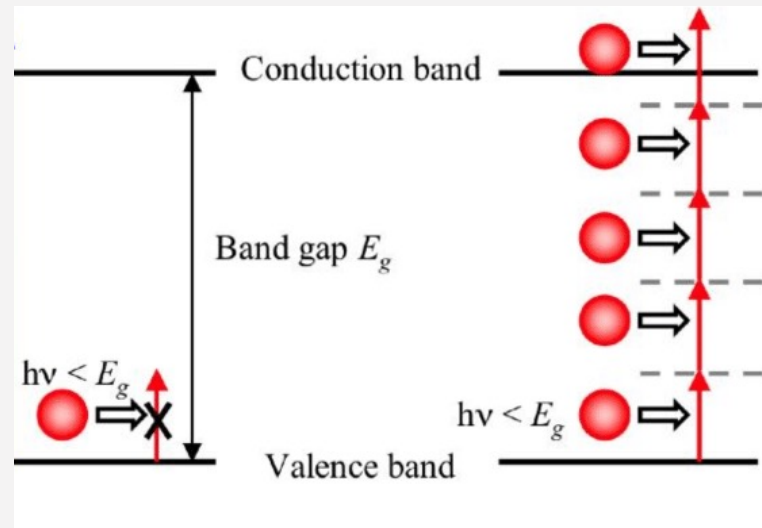
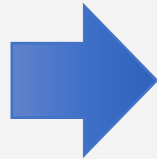
- Fluid Pressure \ll Vapor Pressure
(Constant)



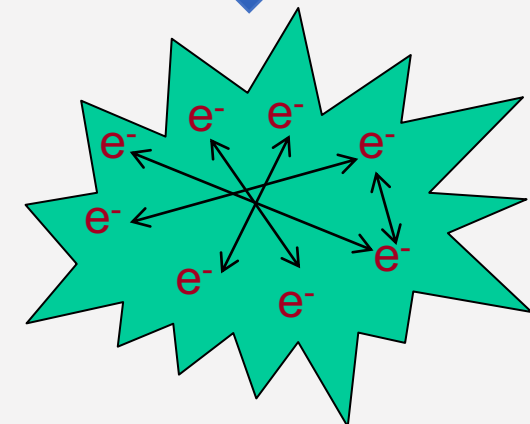
Photoionization (nanoseconds and shorter pulses)



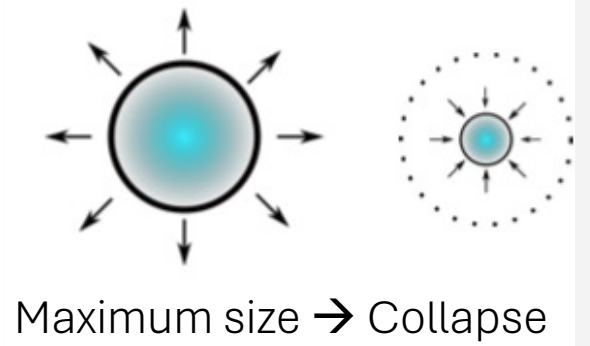
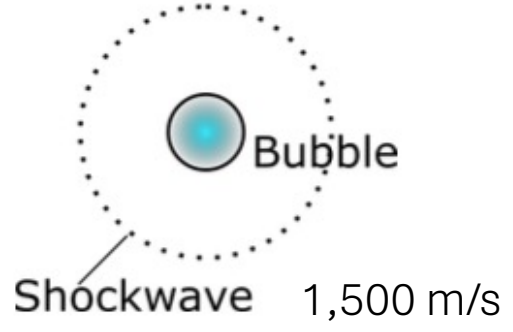
Focused laser beam leads to a high irradiated volume



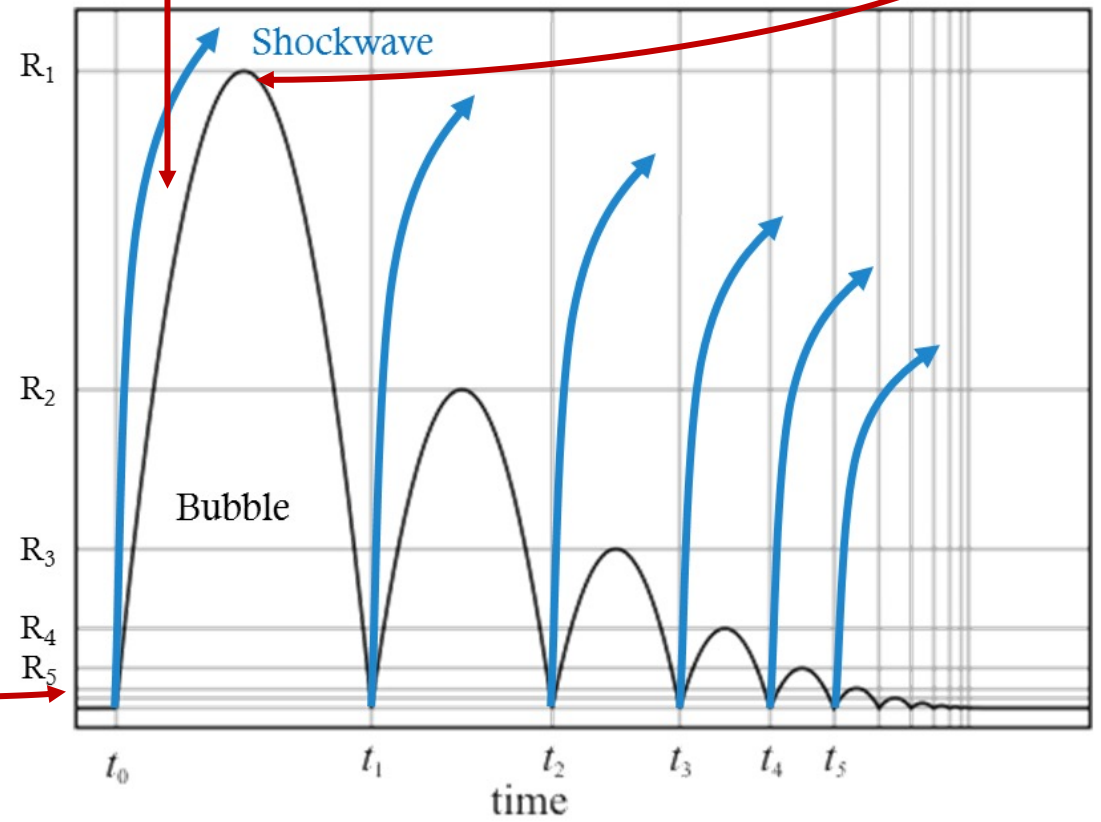
Critic density
 $N > 10^{21} \text{ cm}^{-3}$



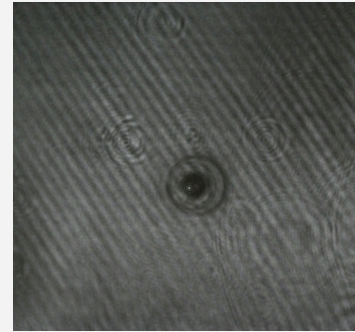
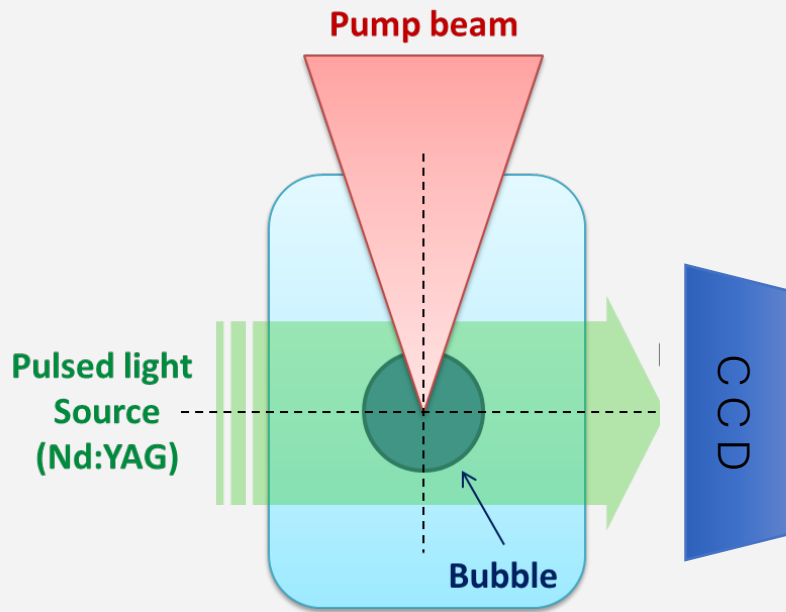
Microexplosi3n



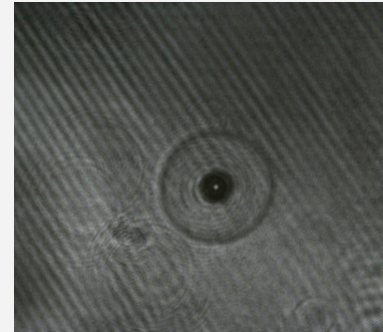
- 2-6GPa, 6000-15,000K¹
- ~10ns duration, ~100μm size²



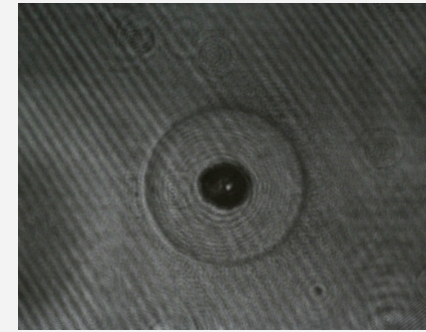
Laser shadowgraphy [750 μ J]



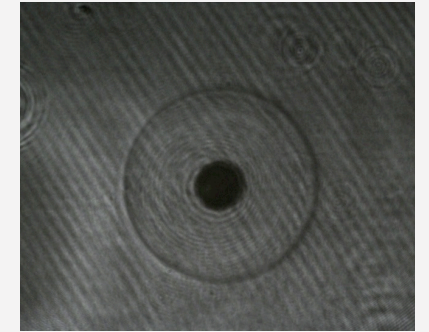
18 ns



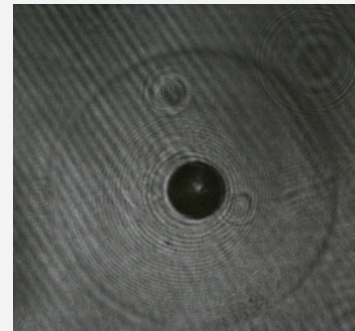
55 us



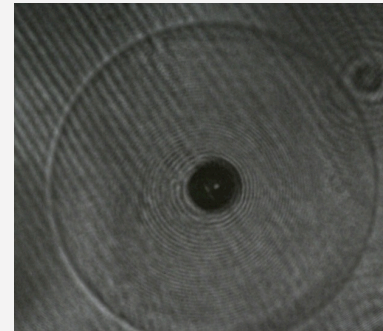
76 us



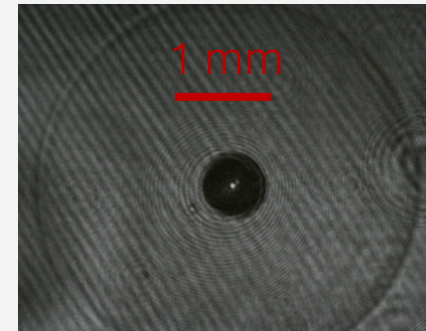
100 us



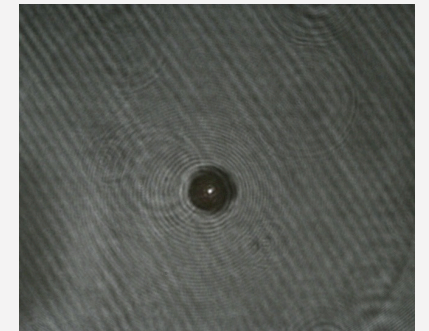
163 us



188 us

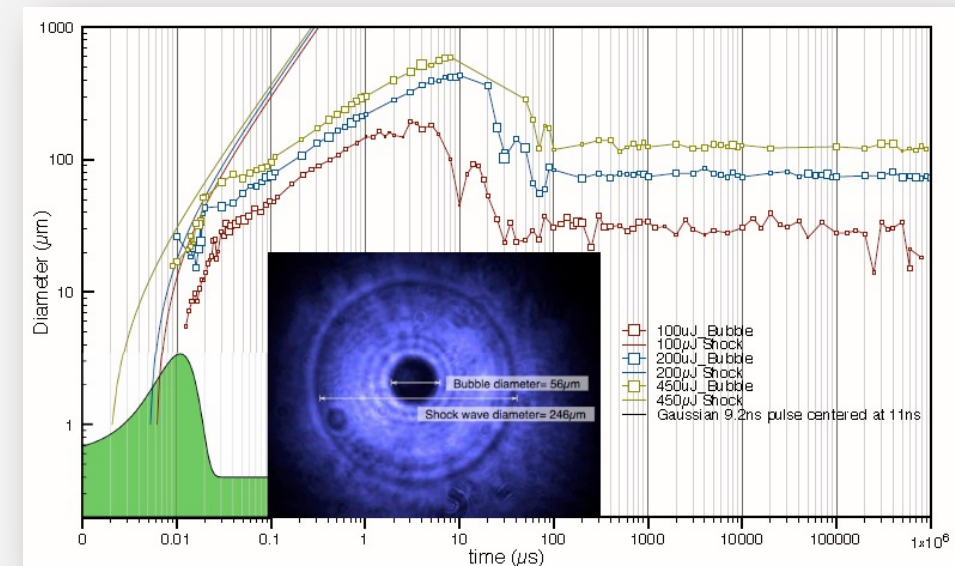
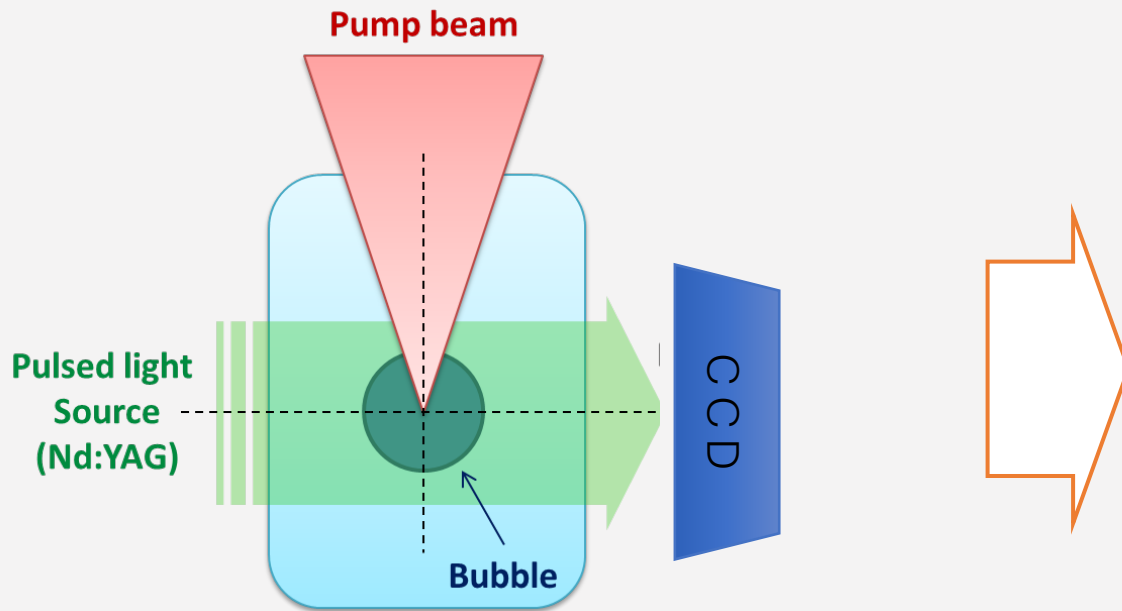


229 us



272 us

Cavitation bubble dynamics reconstruction by Laser Shadowgraphy.



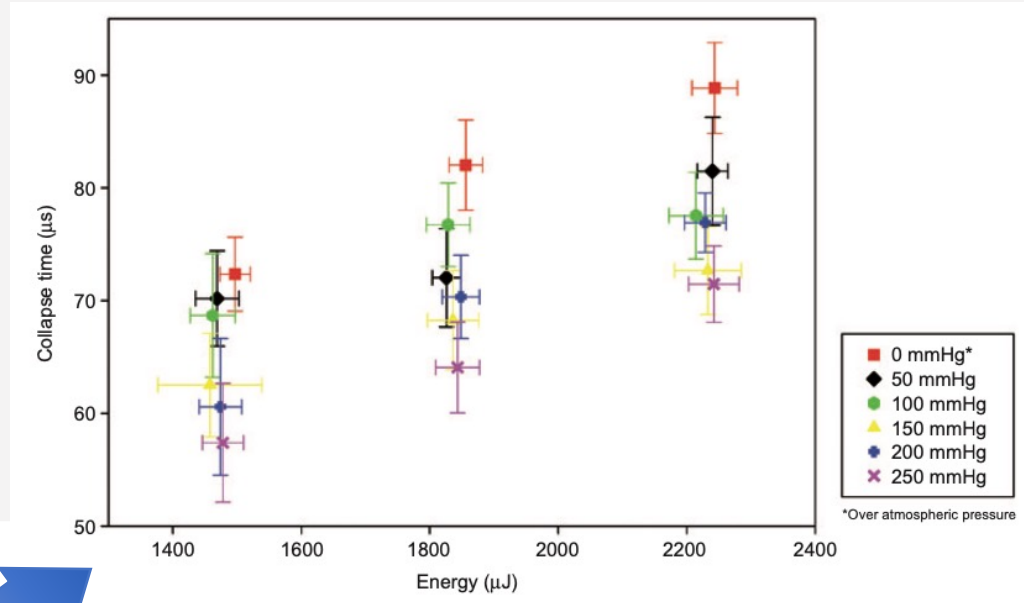
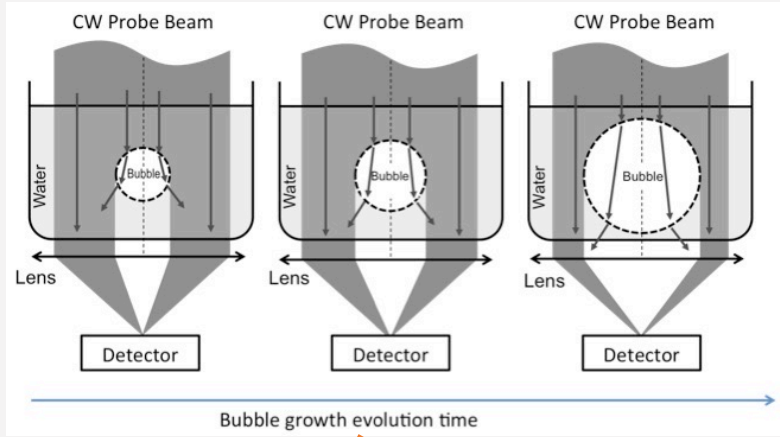
Laser induced cavitation bubble: studies from 2012 to 2023

Article

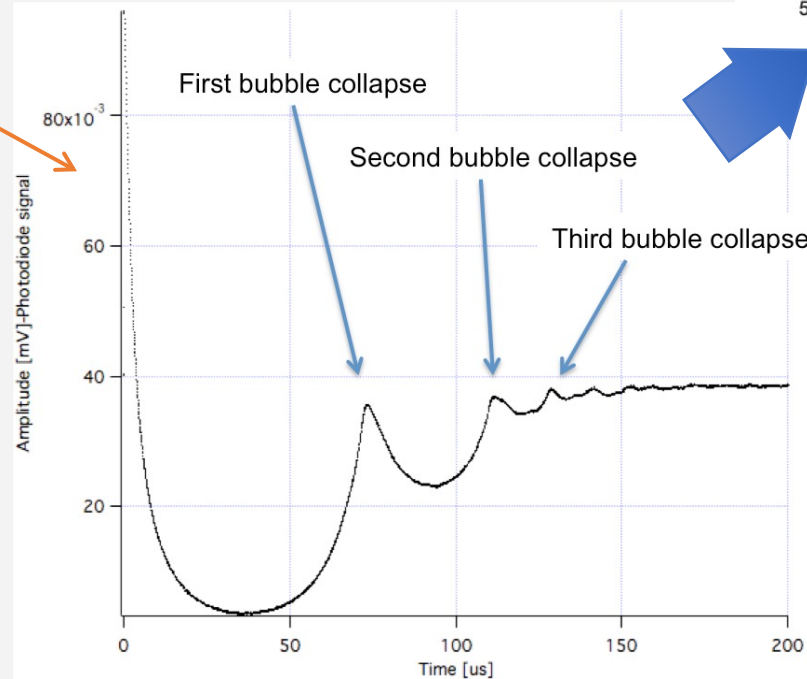
Intraocular Pressure Study in Ex Vivo Pig Eyes by the Laser-Induced Cavitation Technique: Toward a Non-Contact Intraocular Pressure Sensor

Santiago Camacho-Lopez ¹ , Carlos Andrés Zuñiga-Romero ¹, Luis Felipe Devia-Cruz ^{2,*} ,
Carolina Alvarez-Delgado ³ , Marcos Antonio Plata-Sanchez ¹ and Leopoldo Martinez-Manuel ¹

Results

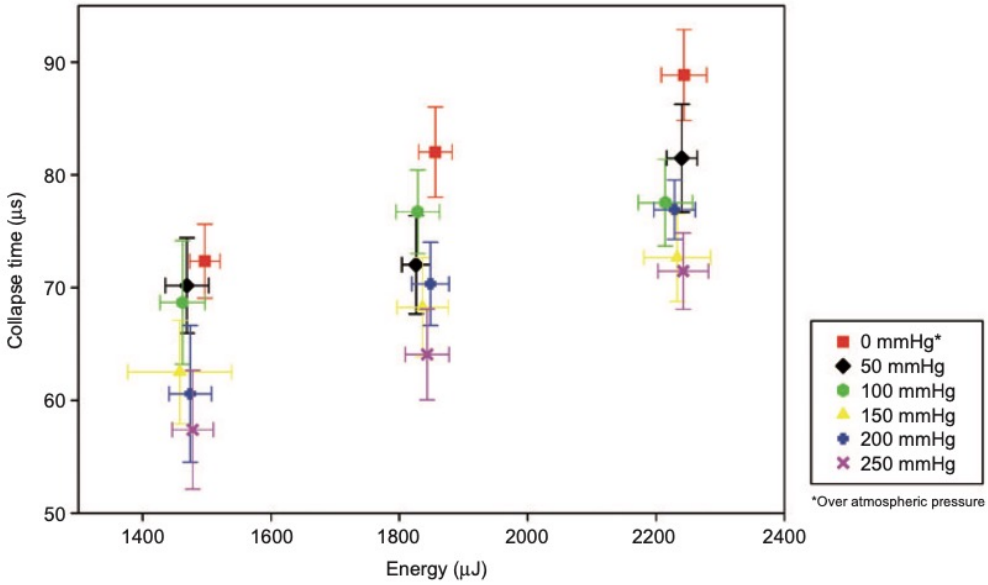


Intensidad medida

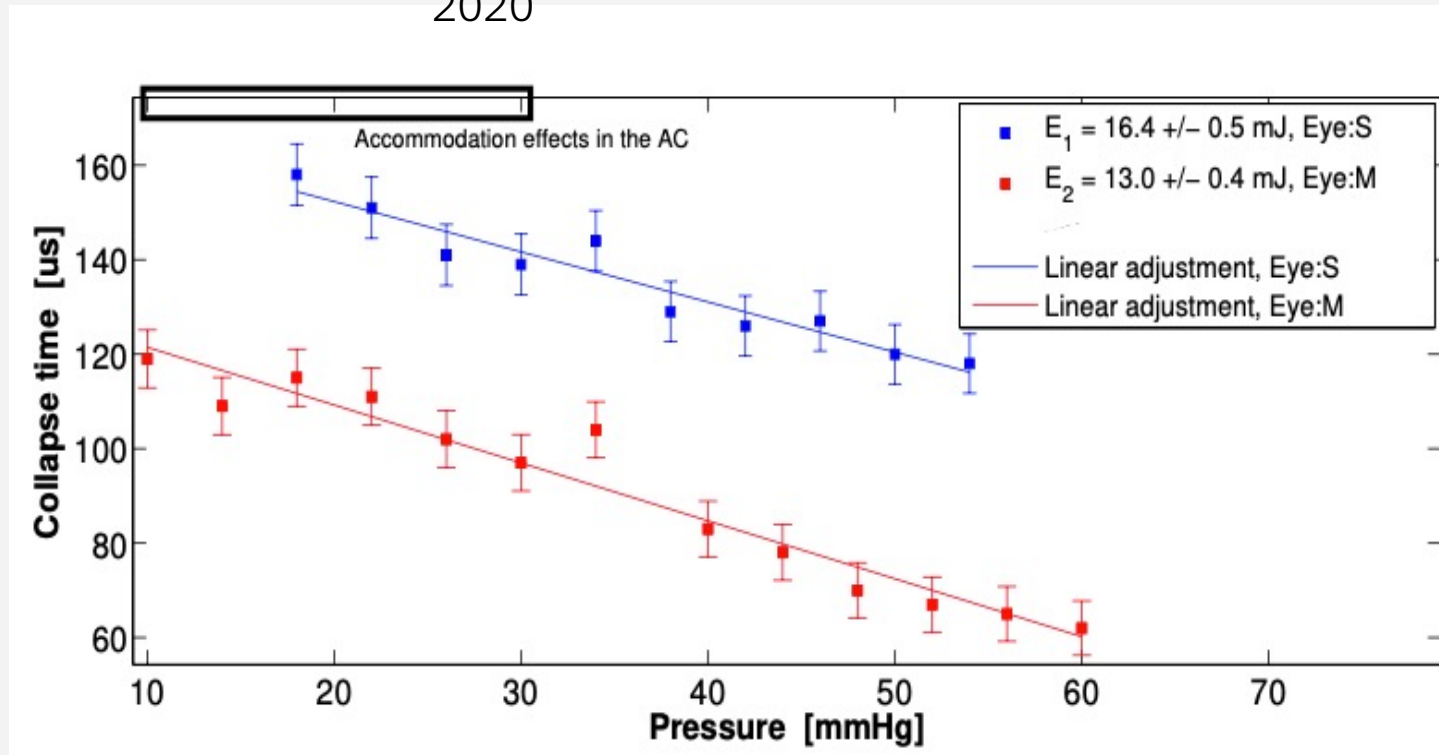


Results

2012



2020

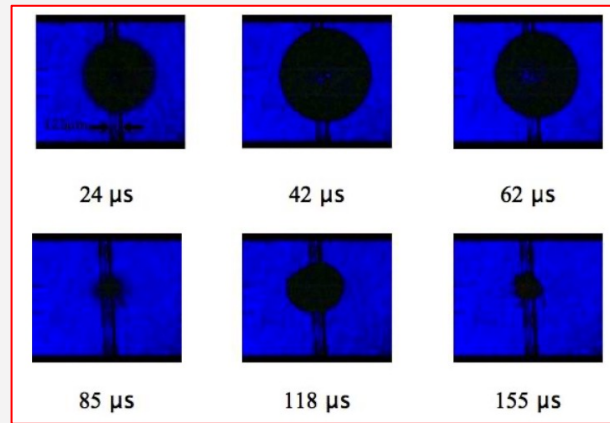
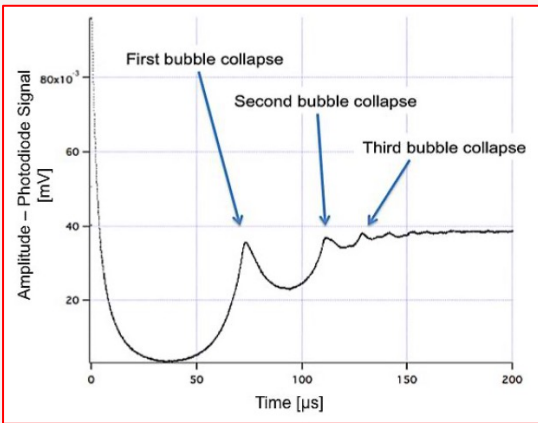
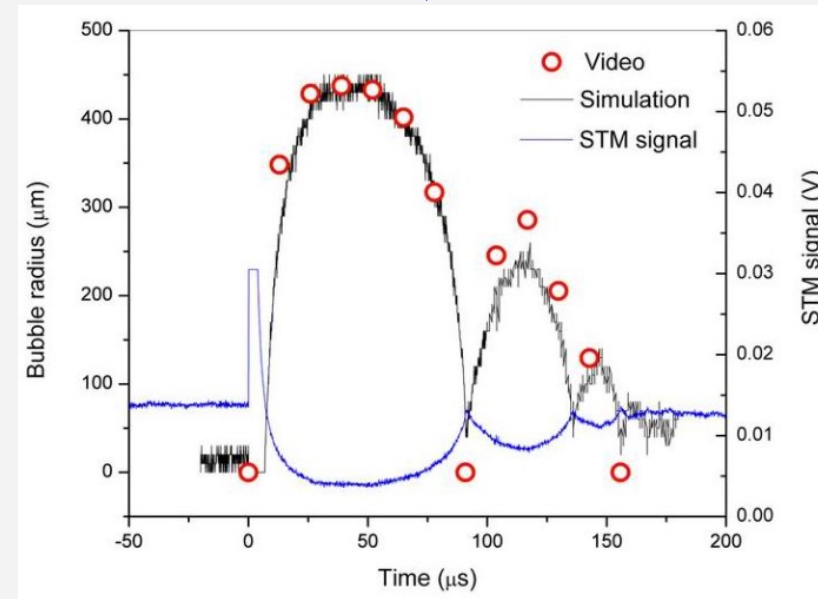
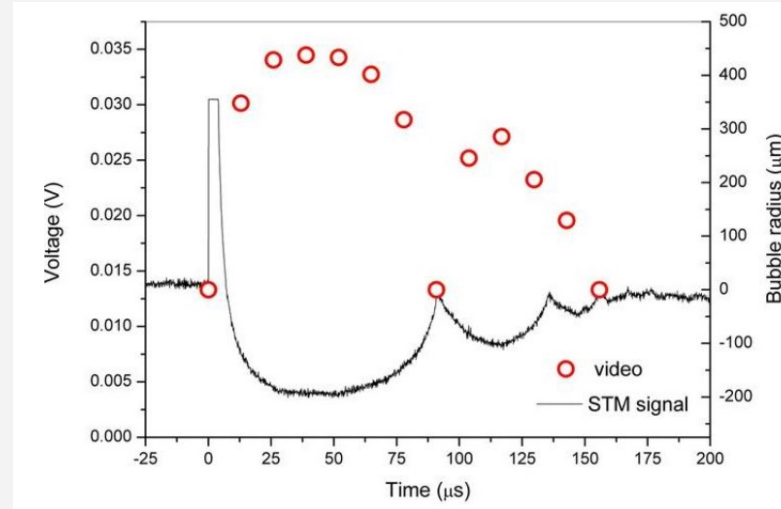


HIGH RESOLUTION OPTICAL EXPERIMENTAL TECHNIQUE FOR COMPUTING PULSED LASER-INDUCED CAVITATION BUBBLE DYNAMICS IN A SINGLE SHOT

Luis Felipe Devia-Cruz,^{1,} Francisco G. Pérez-Gutiérrez,²
Daniel García-Casillas,³ Guillermo Aguilar,³ Santiago
Camacho-López,¹ & Darren Banks³*

Results

$$STMt = \frac{\int_{-w}^w e^{-r^2/2w^2} dr - \int_{-rp}^{rp} e^{-r^2/2w^2} dr}{\int_{-w}^w e^{-r^2/2w^2} dr}$$



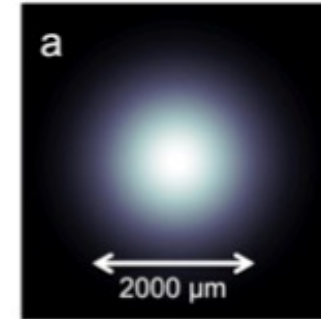
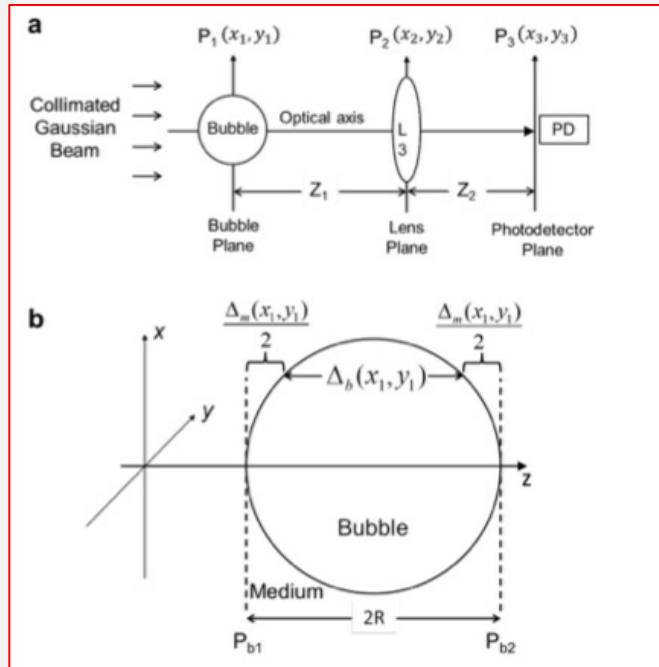
Video de alta Velocidad



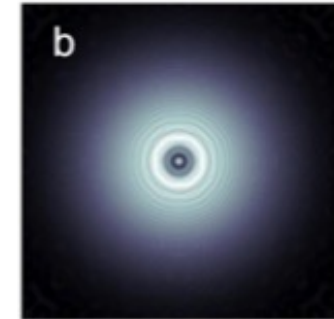
Reconstruction of laser-induced cavitation bubble dynamics based on a Fresnel propagation approach

Luis Felipe Devia-Cruz, Santiago Camacho-López, Víctor Ruiz Cortés, Victoria Ramos-Muñiz, Francisco G. Pérez-Gutiérrez, and Guillermo Aguilar

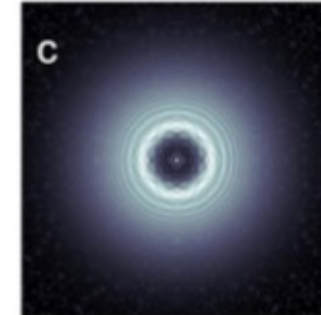
Results



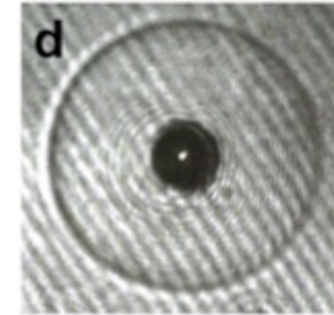
Bubble Radius= 0 μm



Bubble Radius= 100 μm



Bubble Radius= 200 μm



Bubble shadowgraph

$$E(x_2, y_2) = \frac{e^{ikz_1}}{i\lambda z_1} e^{i\frac{k}{2z_1}(x_2^2 + y_2^2)} \mathfrak{S} \left\{ E_b(x_1, y_1) e^{i\frac{k}{2z_1}(x_1^2 + y_1^2)} \right\} \Bigg|_{\substack{f_x = x_2/\lambda z_1 \\ f_y = y_2/\lambda z_1}} \quad (10)$$

Microsystem Technologies (2021) 27:801–812

<https://doi.org/10.1007/s00542-020-04998-0>

TECHNICAL PAPER

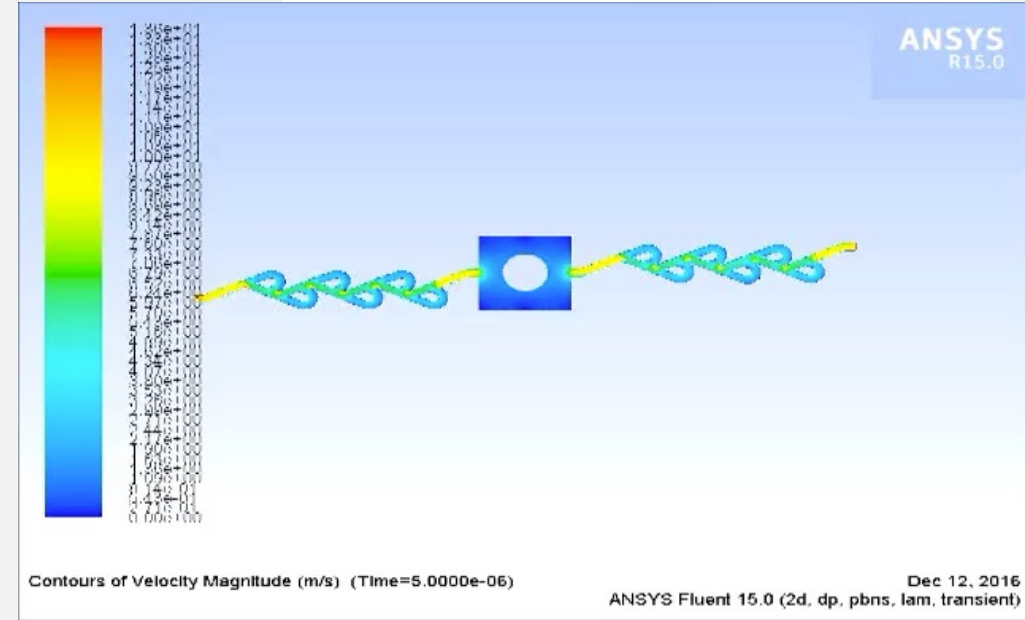
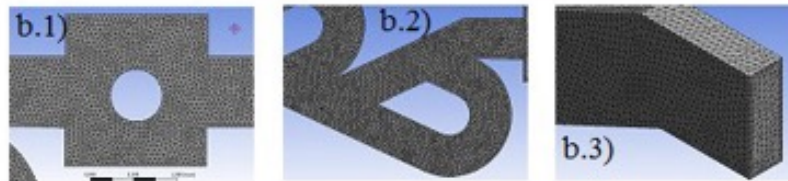
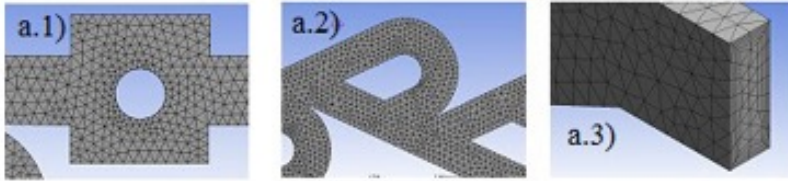
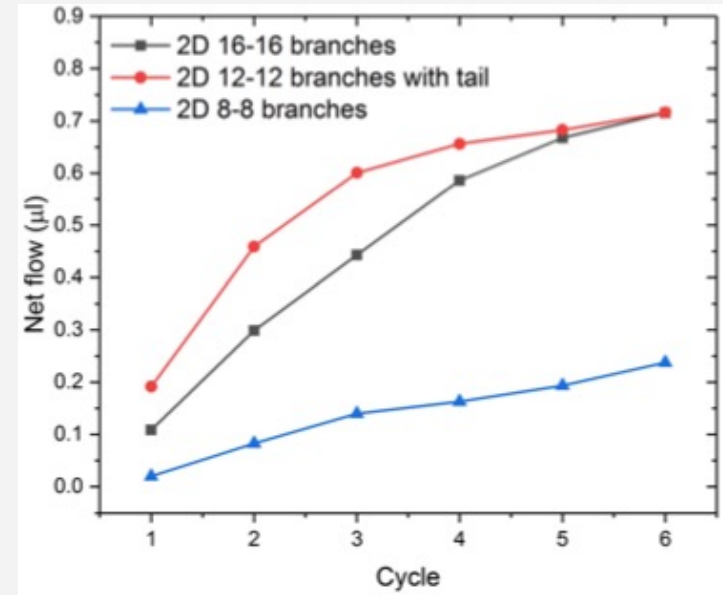
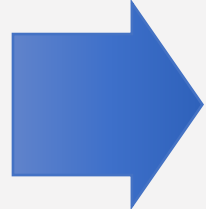
Numerical modeling of a micropump without mobile parts actuated by thermocavitation bubbles

N. G. García-Morales¹ · B. Morales-Cruzado² · S. Camacho-López³ · R. Romero-Méndez¹ ·
L. F. Devia-Cruz³ · F. G. Pérez-Gutiérrez¹ 

Received: 3 June 2020 / Accepted: 8 August 2020 / Published online: 20 August 2020

© Springer-Verlag GmbH Germany, part of Springer Nature 2020







Results



Soft material perforation via double-bubble laser-induced cavitation microjets

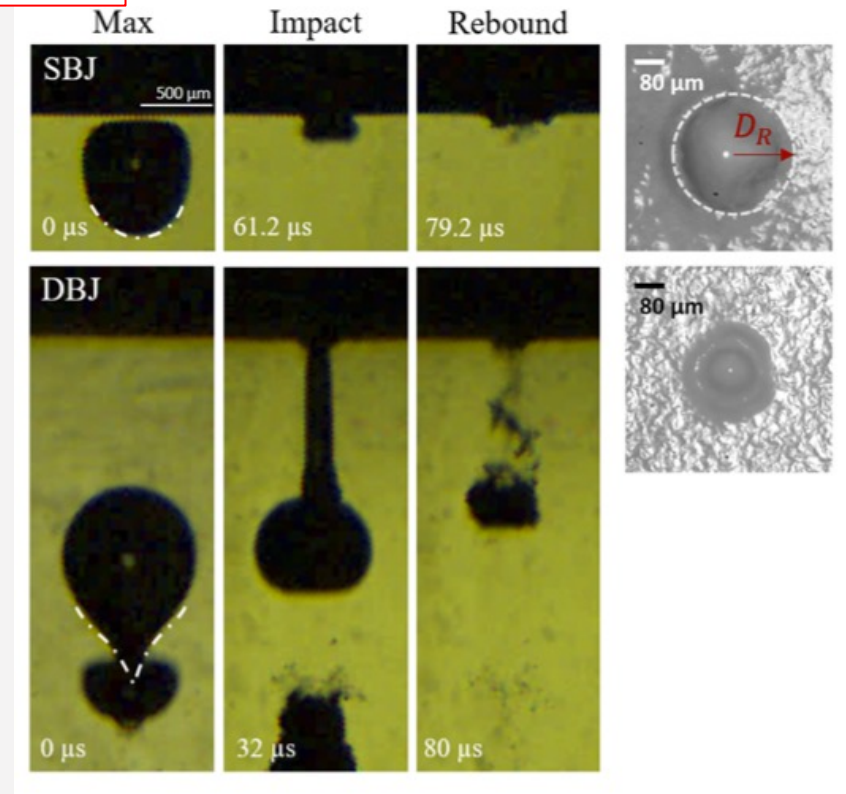
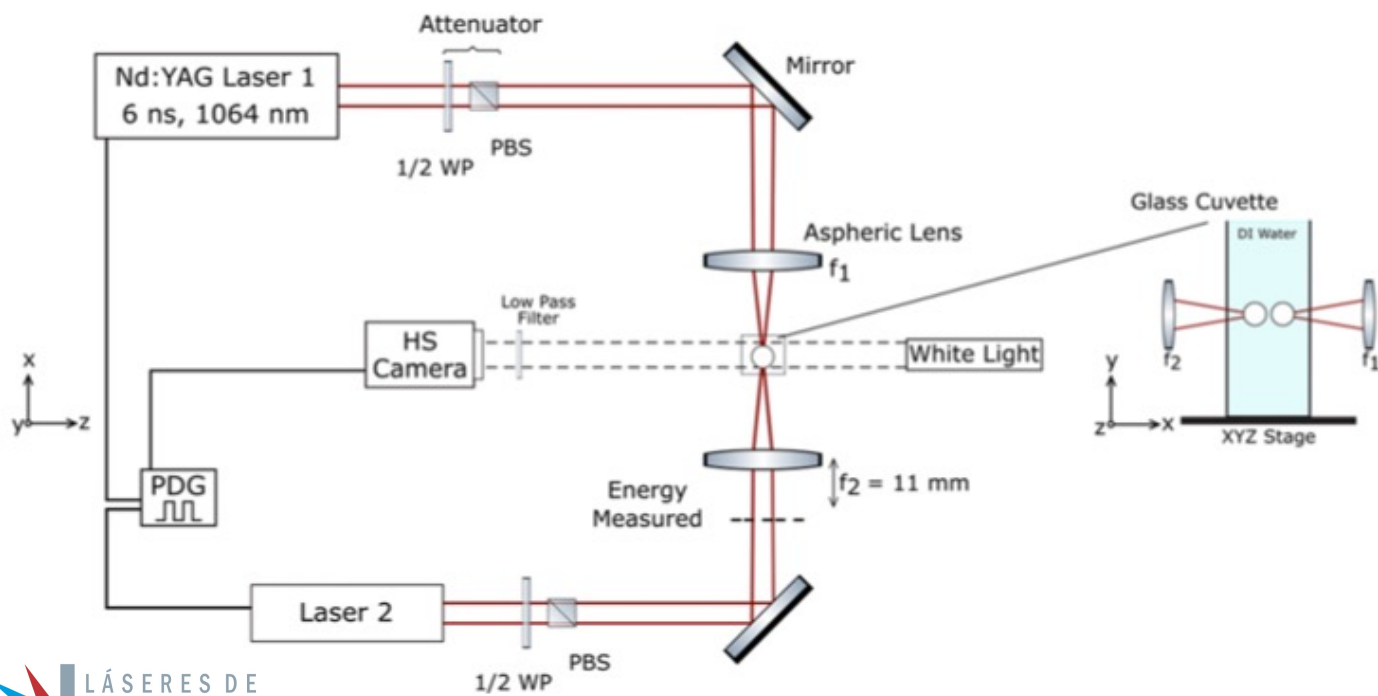
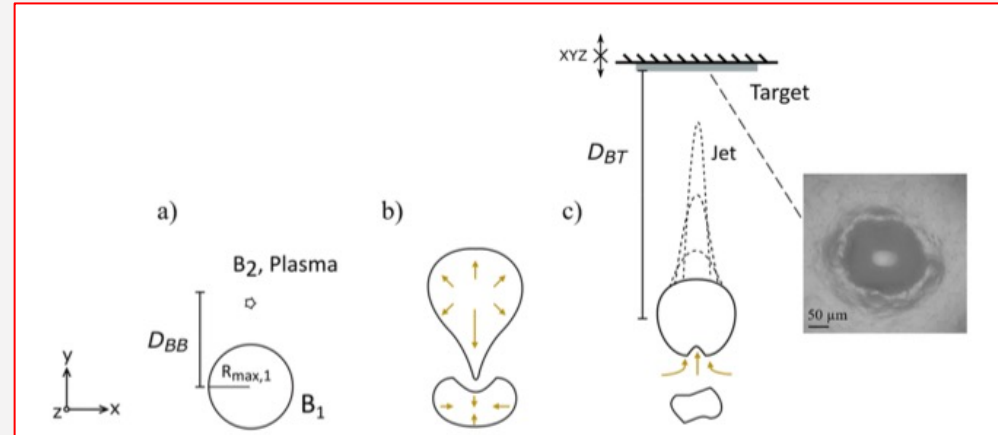
Cite as: Phys. Fluids **32**, 042005 (2020); <https://doi.org/10.1063/5.0007164>

Submitted: 09 March 2020 . Accepted: 02 April 2020 . Published Online: 22 April 2020

V. Robles , E. Gutierrez-Herrera , L. F. Devia-Cruz , D. Banks , S. Camacho-Lopez , and G. Aguilar 



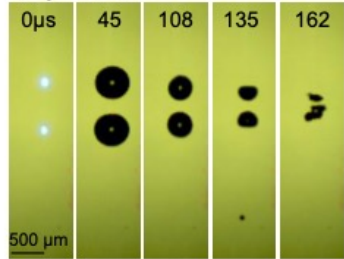
Results



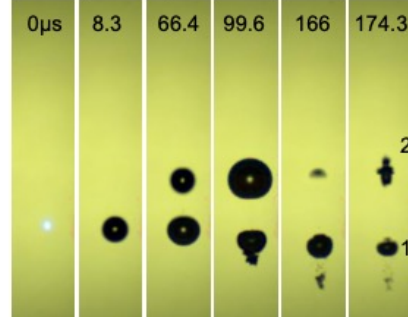
Results

Impinging Jets at Standoff distance

In-phase

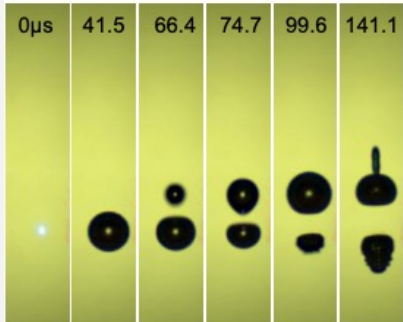


Anti-phase, 0.86

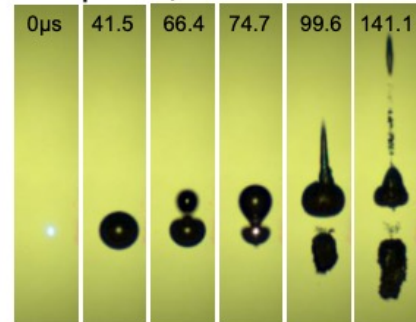


$$\gamma = \frac{D}{(R_{max1} + R_{max2})}$$

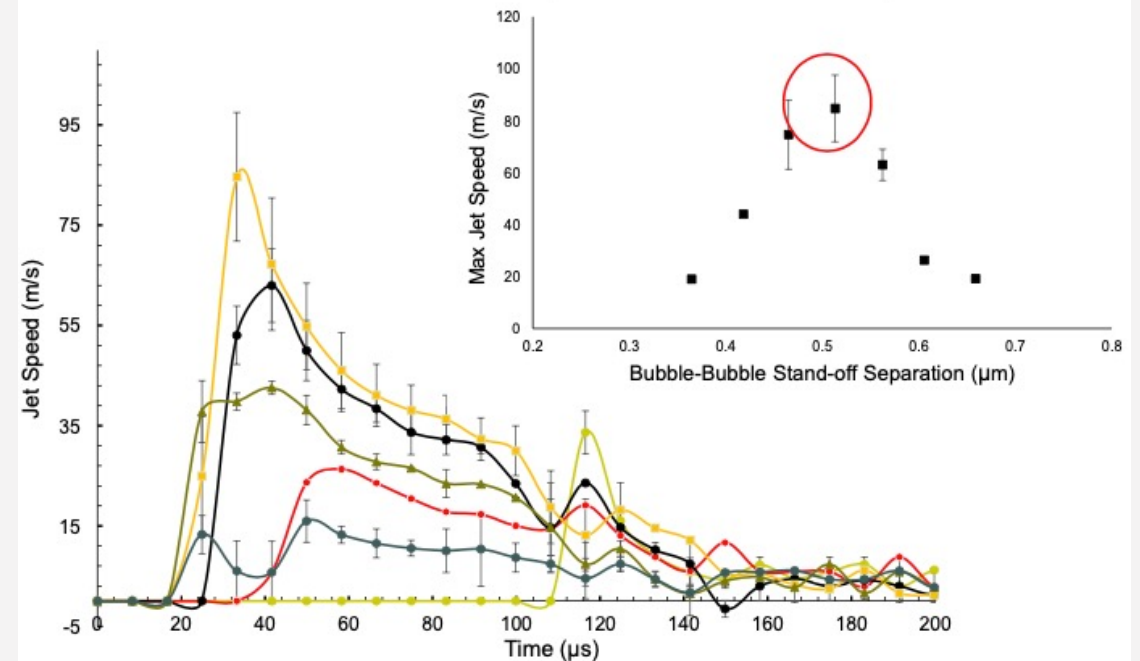
Anti-phase, 0.6



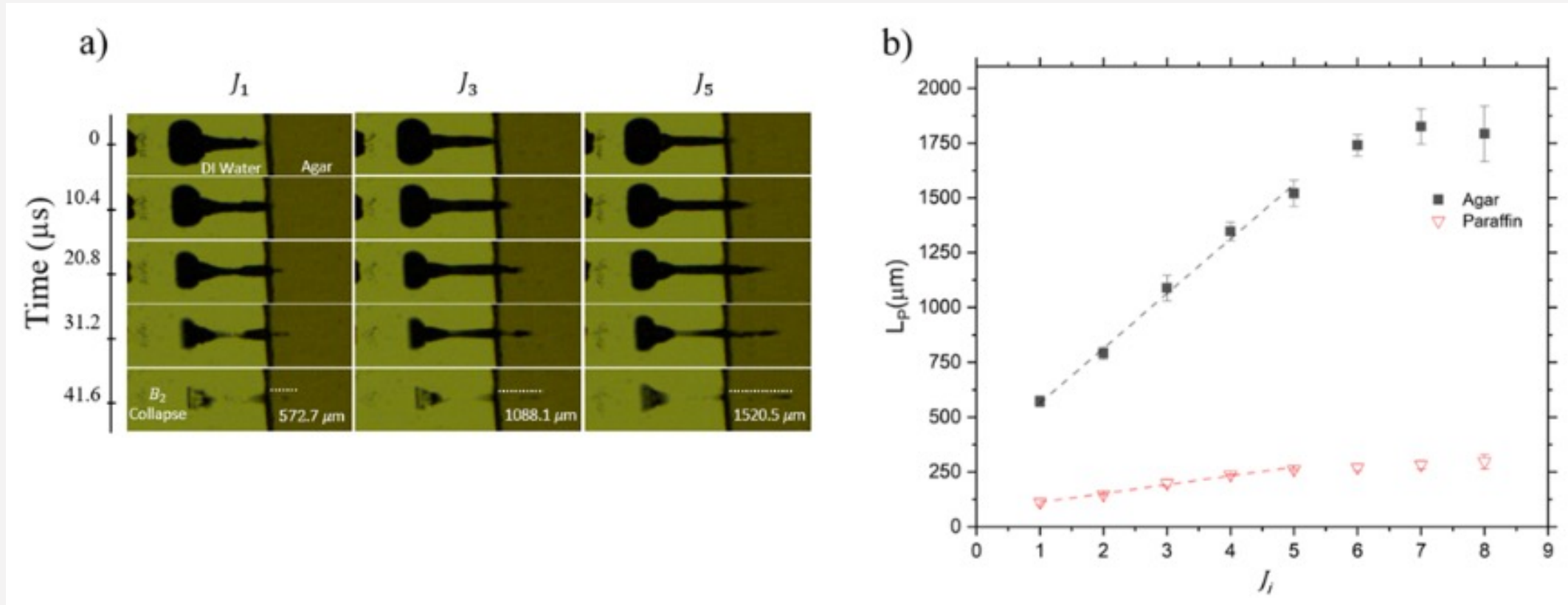
Anti-phase, 0.51



Relative Bubble Separation on Speed



Results





ELSEVIER

Contents lists available at [ScienceDirect](https://www.sciencedirect.com)

Surfaces and Interfaces

journal homepage: www.sciencedirect.com/journal/surfaces-and-interfaces

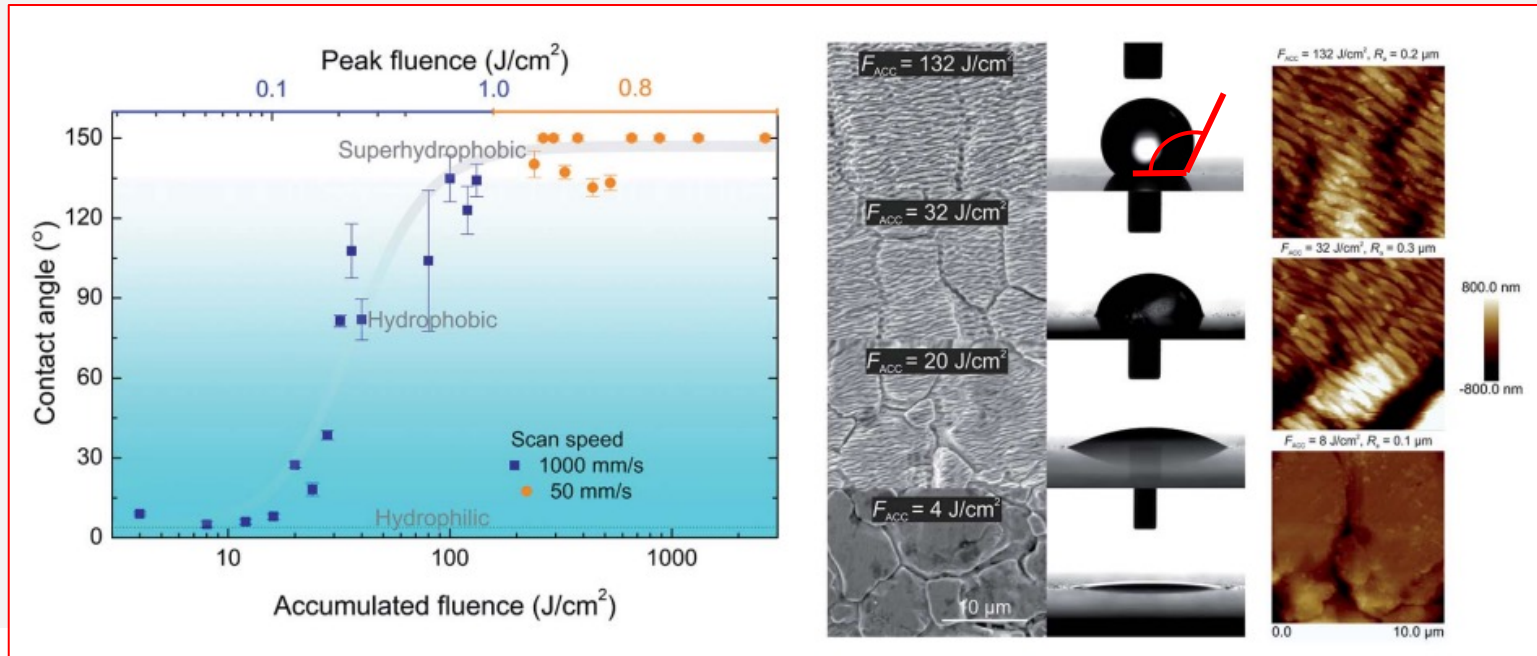
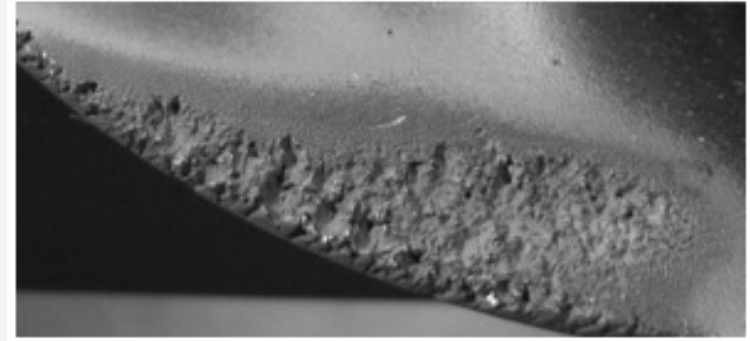
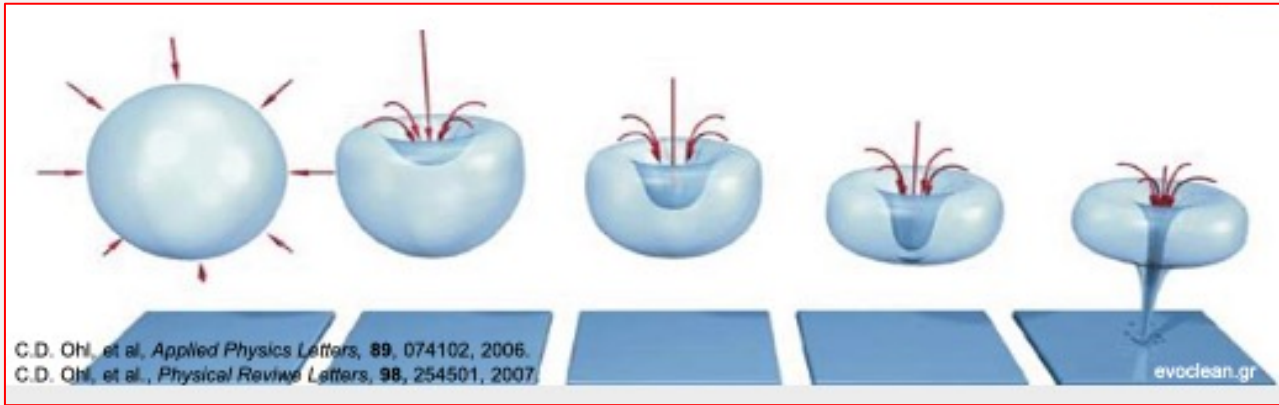
Mitigation of cavitation erosion using laser-induced periodic surface structures

Juan Carlos Gonzalez-Parra^a, Vicente Robles^a, Luis Felipe Devia-Cruz^b,
Rene I. Rodriguez-Beltran^b, Natanael Cuando-Espitia^{c,*}, Santiago Camacho-Lopez^{b,*},
Guillermo Aguilar^{a,*}

^a Department of Mechanical Engineering, University of California Riverside, CA, United States

^b Departamento de Óptica, Centro de Investigación Científica y de Educación Superior de Ensenada, Ensenada, México

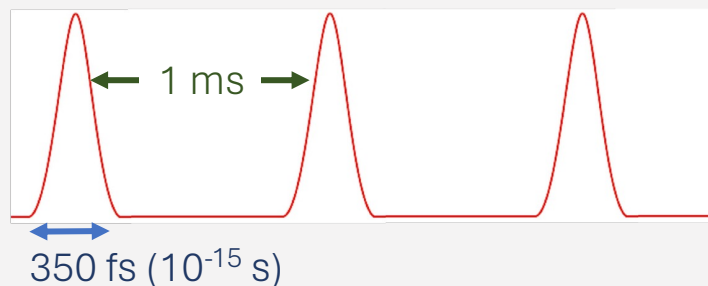
^c CONACyT, Applied Physics Group, DICIS, University of Guanajuato, Salamanca, Guanajuato 368850, Mexico



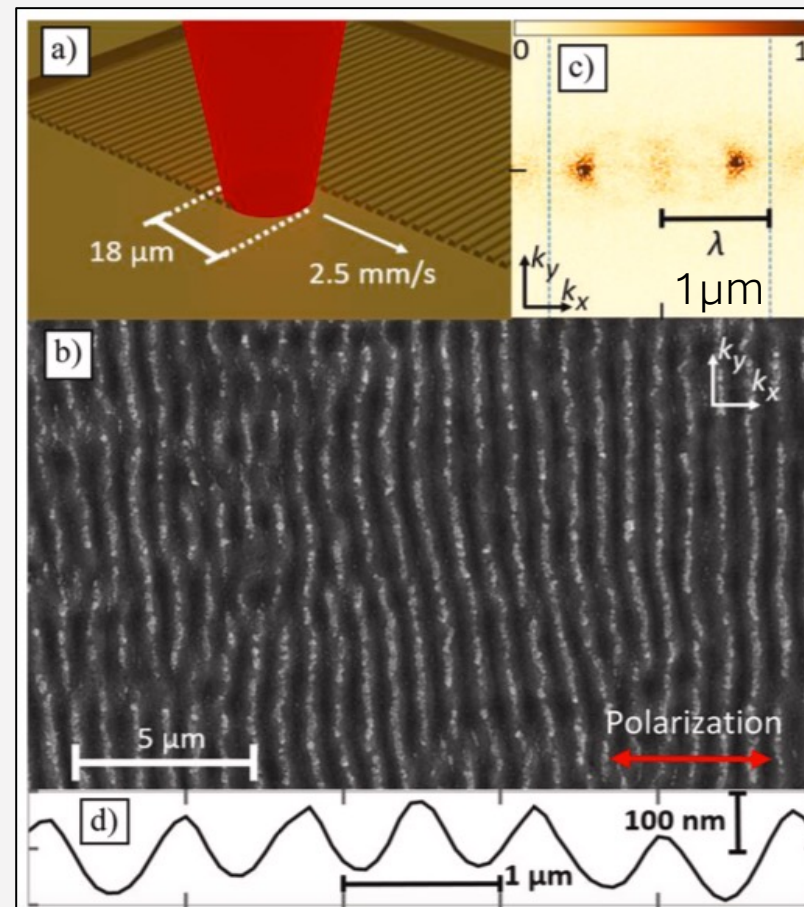
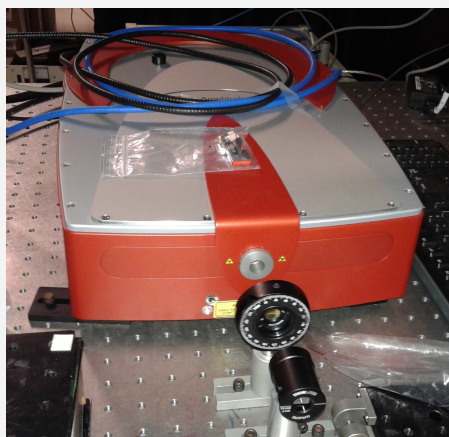
Andrius Žemaitis *et al.* Controlling the wettability of stainless steel. <https://doi.org/10.1039/D0RA05665K>

Laser patterning of the surface

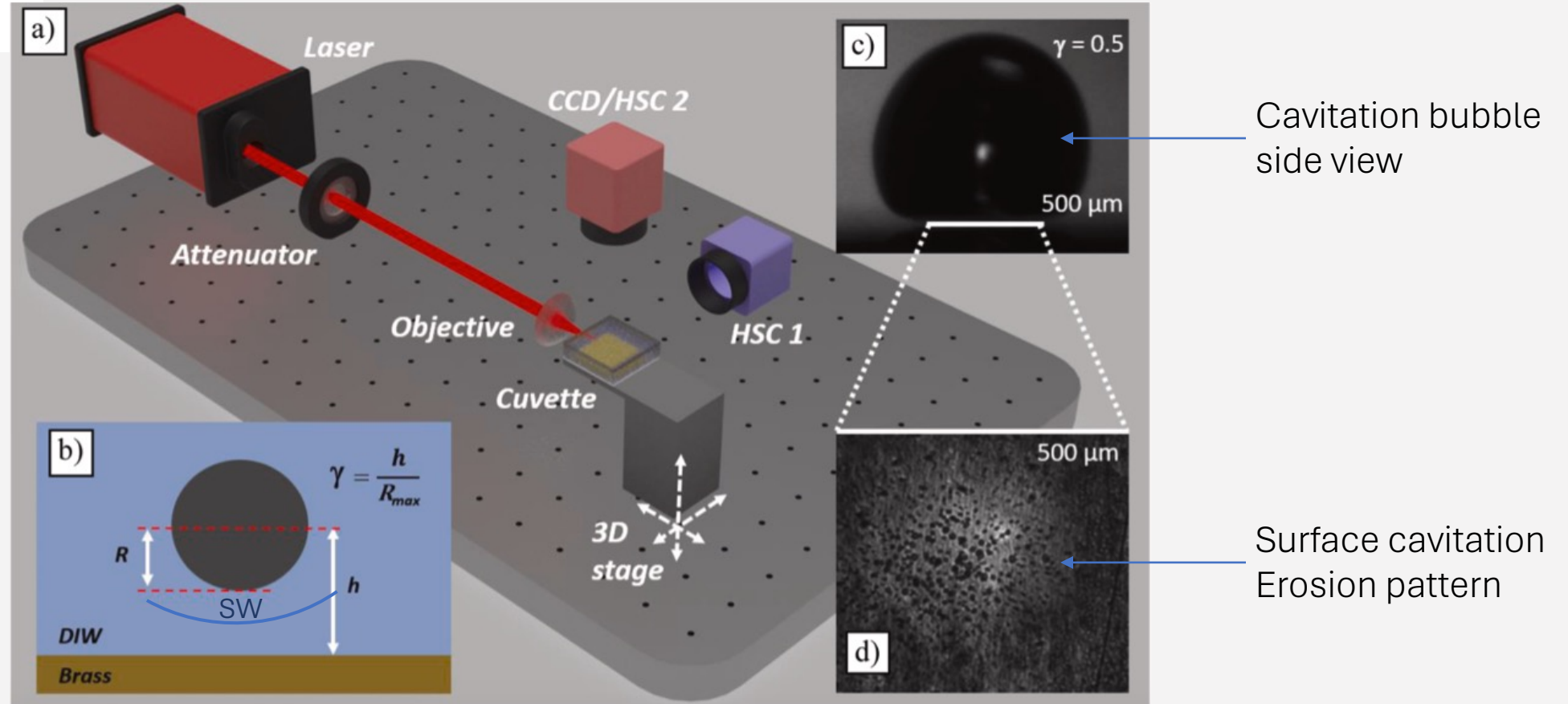
Ablation threshold = 0.9 J/cm^2



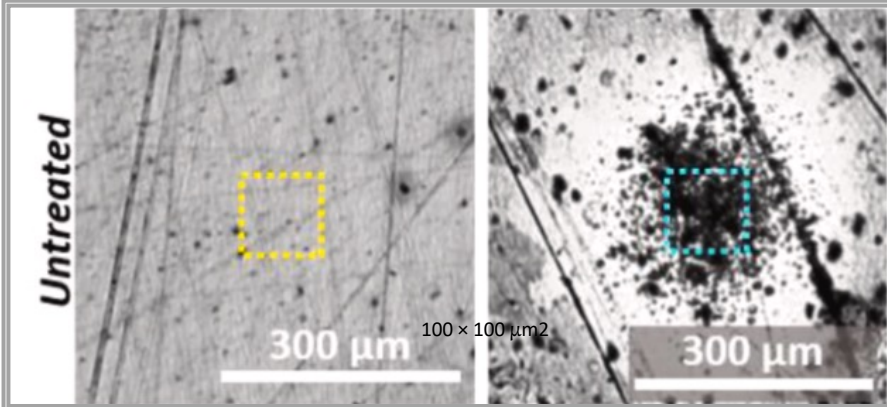
Beamwaist [$1/e^2$]: $18 \mu\text{m}$
Wavelength: 1030 nm
Per pulse energy: $27 \mu\text{J}$
Repetition rate: 1 kHz
Speed: 2.5 mm/s
Fluence: 0.78 J/cm^2
Pitch: $22 \mu\text{m}$



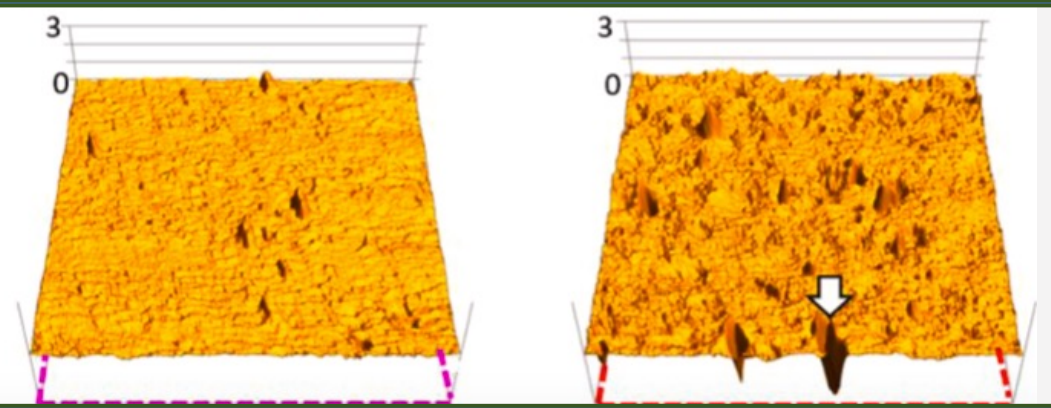
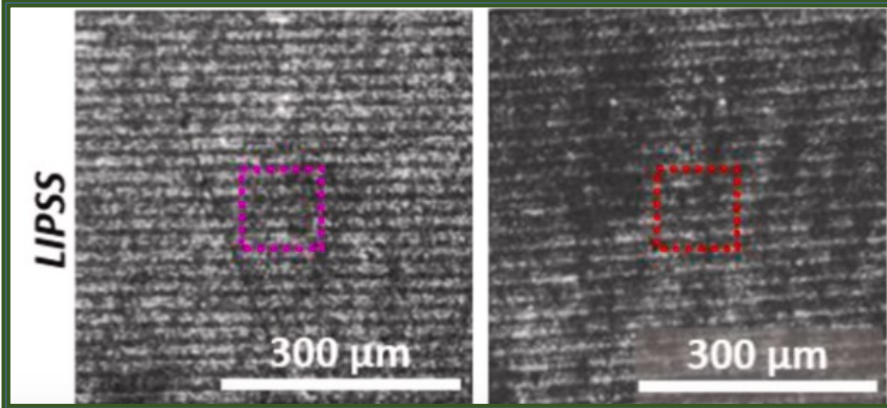
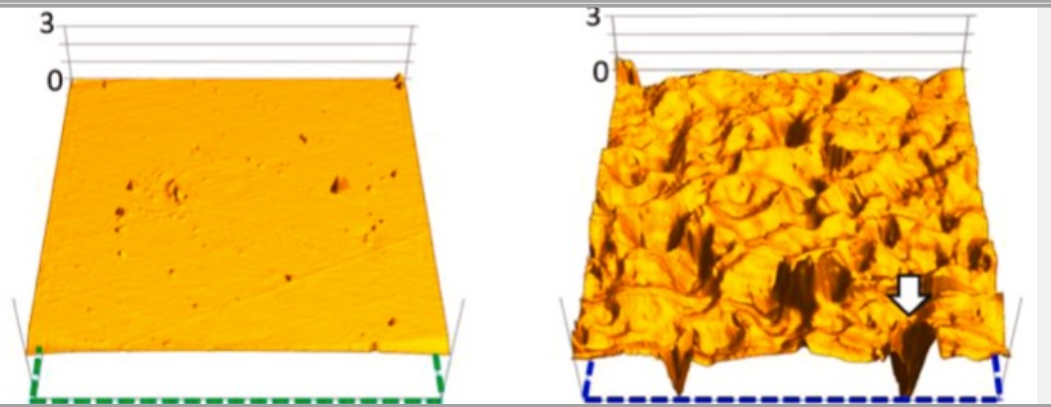
Erosion test through laser-induced cavitation



Before cavitation After 200k cavitation events



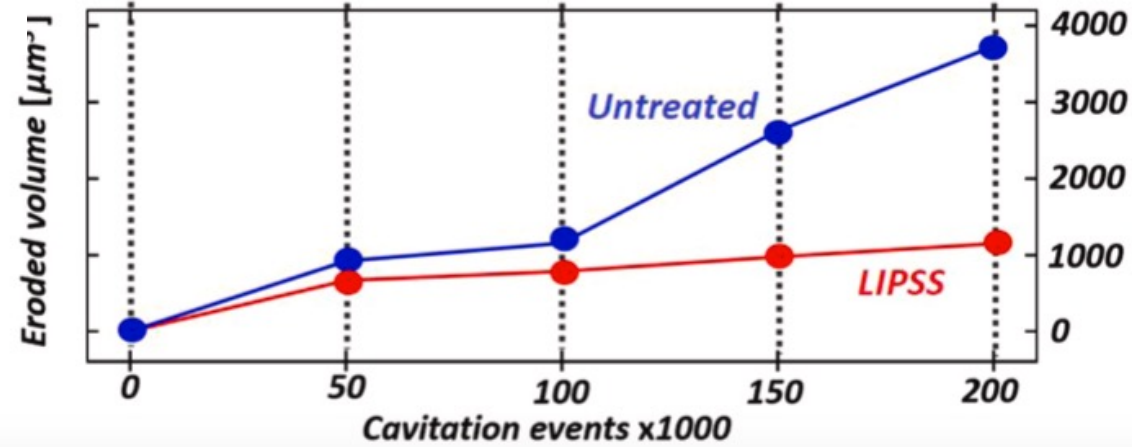
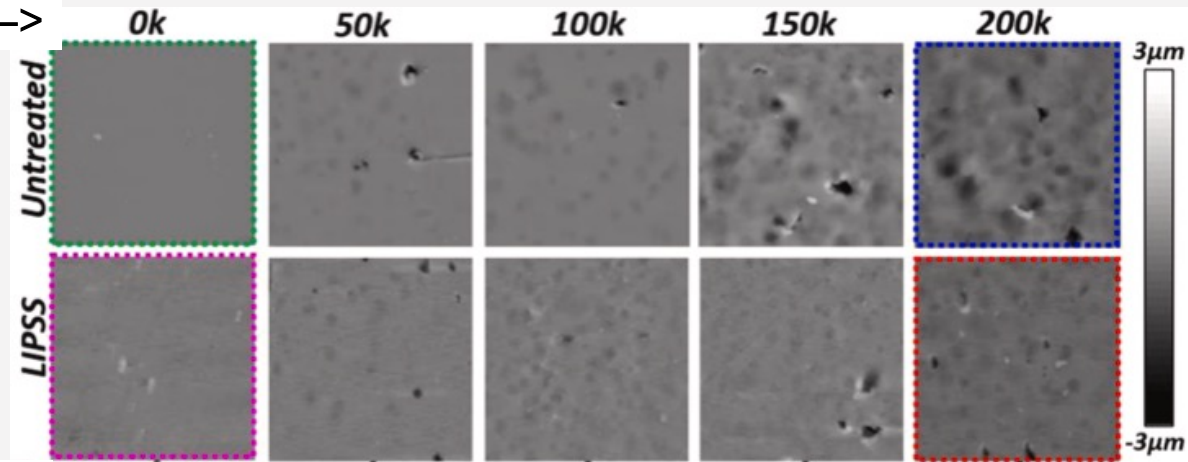
Before cavitation After 200k cavitation events



100 μm

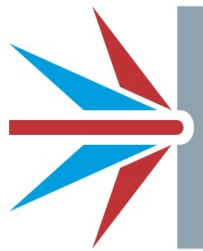
Results

Number of cavitation events →



Final Remarks

Gracias por su atención
ldevia@cicese.mx



LÁSERES DE
PULSOS ULTRACORTOS
Y PROCESAMIENTO DE MATERIALES